ORIGINAL PAPER-EXPLORATION GEOPHYSICS

Geophysical appraisal for the sandy levels within Abu Roash C and E members in Abu Gharadig Field, Western Desert, Egypt

Mohammad Abdelfattah Sarhan[1,2]

Abstract

The present work concerns with the geophysical assessment for the sandstones of Abu Roash C and E members for being potential hydrocarbon reservoirs at Abu Gharadig Field, Western Desert, Egypt. The analysis of seismic data covers Abu Gharadig Field showing ENE–WSW anticline fragmented by NW–SE normal faults. The presence of these structures is due to the dextral wrench corridor that extensively deformed the north area of the Western Desert within Late Cretaceous episode. The examination of well-log data of Abu Gharadig-6 Well revealed that the favourable zone locates between depths 9665–9700 ft (zone I) within Abu Roash "C" Member. The second promising zone in Abu Gharadig-15 Well occurs between depths 9962–9973 ft (zone II) in Abu Roash "E" Member. The quantitative evaluation indicated that zone I has better reservoir quality than zone II since it is characterised by low shale volume (0.01), high effective porosity (0.22), low water saturation (0.14), low bulk volume of water (0.03), higher values of absolute permeability (113 mD), high relative permeability to oil and low water cut, whereas zone II has 0.13 shale volume, 0.16 effective porosity, 0.39 water saturation, 0.06 bulk volume of water, lower values of absolute permeability (27 mD), low relative permeability to oil and relatively high water cut. The obtained results recommended that the drilling efforts should be focused on the sandy levels within Abu Roash C Member (1st priority) and the sand levels within Abu Roash E Member (2nd priority) in Abu Gharadig Basin and its surroundings.

Keywords Seismic interpretation · Well logging · Abu Roash formation · Abu Gharadig Field

Introduction

Abu Gharadig Basin (AG Basin) is the largest sedimentary basin in the northern Western Desert of Egypt (Fig. 1). It is an intra-cratonic E-W rift basin of approximately 330 km long and 50 to 75 km wide (El Gazzar et al. 2016). AG Basin has attracted the attention of several geoscientists (e.g. Abd El Aal 1988; El Sayed et al. 1993; El Diasty and Moldowan 2012; Sarhan 2017a,b,c, 2020; Barakat and Nooh 2017; Sarhan and Collier 2018; Hewaidy et al. 2018; Elmahdy et al. 2020; El-Bagoury 2020).

AG Basin has a huge subsurface sedimentary sequence of Jurassic up to Tertiary deposits. The Jurassic and Cretaceous sediments include the main source rocks generating petroleum in AG Basin (Shahin 1992). The Cenomanian Bahariya Formation plus the Turonian-Coniacian Abu Roash Formation hold over 90% of the petroleum reserves in Western Desert region (Richardson et al. 1998).

The oil of AG Basin is commonly produced from structural traps attributed to the Syrian Arc tectonic (e.g. Abu El Naga 1984; Dolson et al. 2001; Moustafa 2008). These traps show three- or four-way structural closures in addition to the fault block structures mostly the NE-SW and NW–SE faults (Abd El Aal 1988; Sultan and Abd El Halim 1988).

Abu Roash Formation represents a potential hydrocarbon reservoir in AG Basin even from its clastic or carbonate members (El Gezeery and O' Connor 1975; Sestini 1995). The fractured limestones of Abu Roash D Member are an important hydrocarbon reservoir in Gindi Basin (Sarhan et al. 2017), while Abu Roash F Member is the supreme oil-prone source rock in Gindi Basin (Sarhan and Basal 2020) and in AG Basin (EGPC 1992; Labib 1985).

Abu Gharadig Field is the first huge hydrocarbon discovery in AG Basin for oil and gas production (El Gazzar et al. 2016). It is sited in the middle portion of AG Basin between

✉ Mohammad Abdelfattah Sarhan
msarhan@du.edu.eg

1   Geology Department, Faculty of Science, Damietta University, New Damietta City, Egypt

2   Center of Space Research and Applications (CSRA), Damietta University, New Damietta City, Egypt
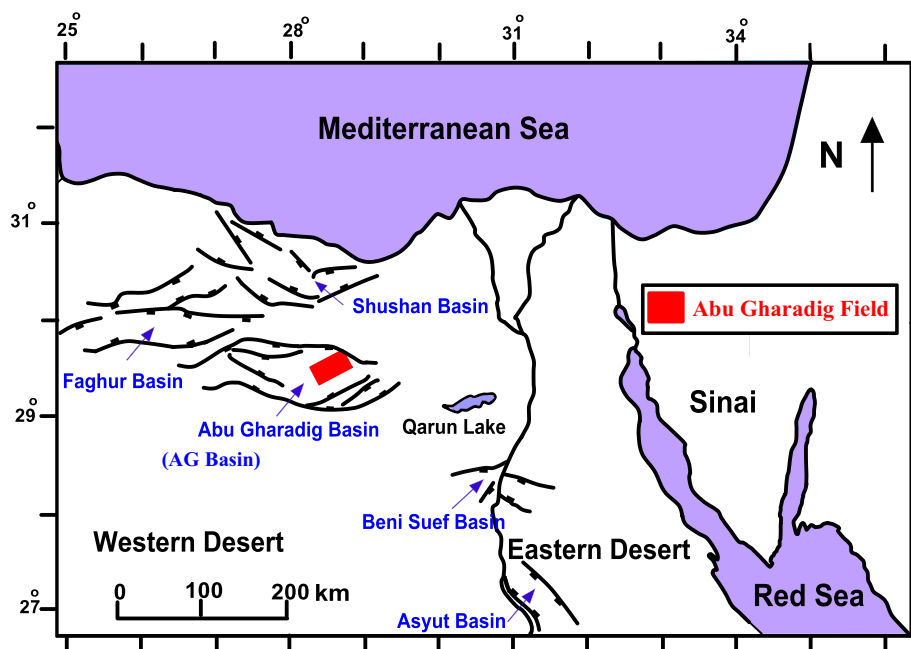
longitudes 28.3° and 28.5° E and latitudes 29.5° and 29.7° N as shown in Fig. 1.

The objective of this study is to assess the hydrocarbon possibility of the sand levels of Abu Roash C and E members in Abu Gharadig Field via the interpretations of the available seismic and well-logs data in the study area.

Geologic setting

AG Basin was originated throughout the Jurassic-Early Cretaceous episode as a rift basin. It was affected by a prevailed sinistral wrenching in Early Cretaceous (Meshref et al. 1988), but in the Late Cretaceous, it was subjected by dextral wrenching caused by the revers in the provincial stress field (e.g. Sarhan 2017b). This reversal stress was due to the move of the African Plate westward comparative to the Laurasian Plate (Smith 1971; Biju-Duval et al. 1977). This dextral wrenching produced NE–SW compressional features such as the Mubarak High and the Abu Gharadig anticline in addition to NW–SE to WNW–ESE extensional normal faults (Barakat and Nooh 2017). This episode ended during the Santonian, which was a period of uplift and erosion due to the move of the African Plate northward (Abd El Aal and Moustafa 1988; Guiraud and Bosworth 1997). This inversion influenced AG Basin till the Early Tertiary time (Moustafa 2008). The inversion formed a series of NE–SW-trending folds, which termed Syrian arc fold system (e.g. Moustafa and Khalil 1990; Moustafa et al. 1998; Moustafa 2002).
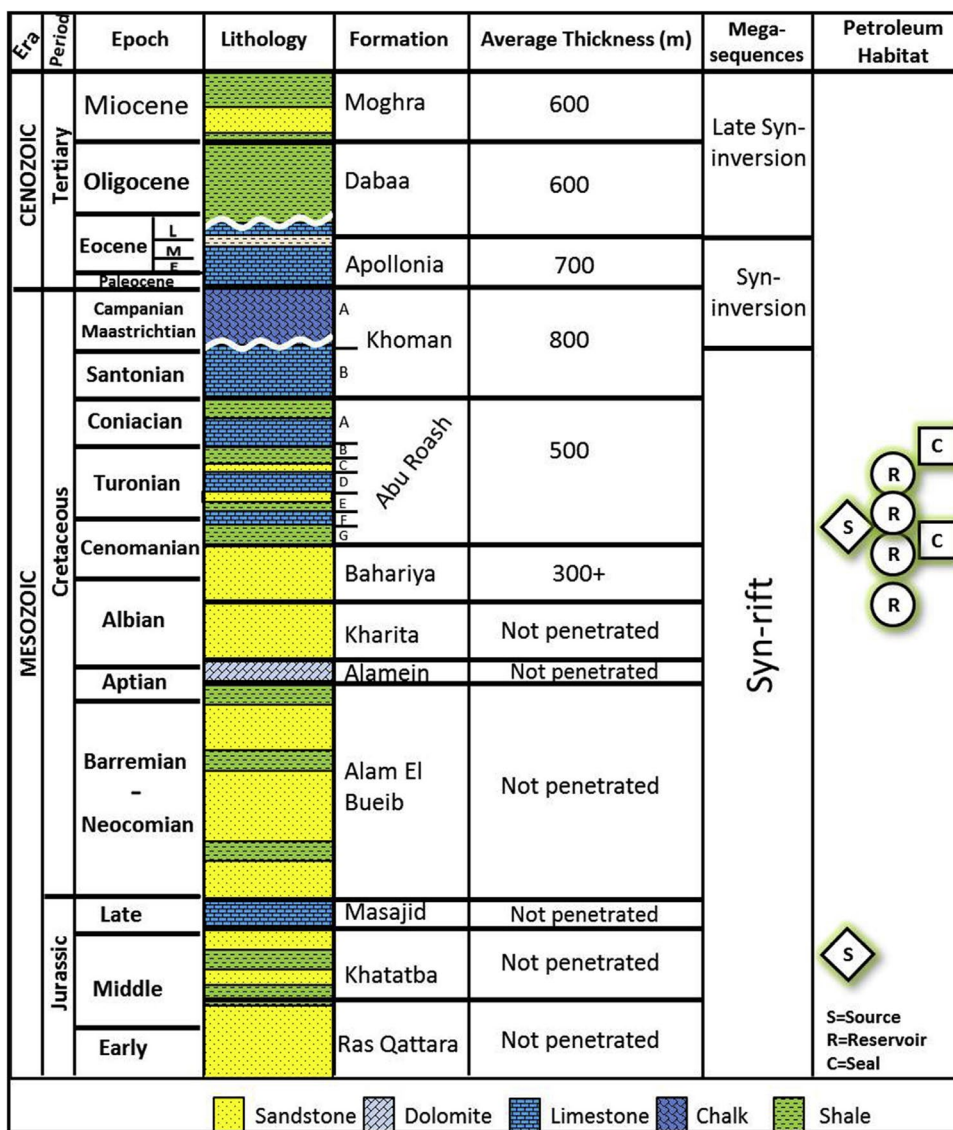
The Turonian–Coniacian Abu Roash Formation overlies the Cenomanian Bahariya Formation and underlies the Santonian–Maastrichtian Khoman Formation (Fig. 2) and composed of alternations between carbonates and clastics deposited in shallow marine setting (EGPC 1992) under fluctuating sea levels (Sarhan 2017a). It is separated into seven members (A, B, C, D, E, F and G) from top to base. The members B, D and F are consisting mainly of limestone deposited in moderately high sea-level intervals, while, A, C, E and G members are siliciclastic in nature and deposited throughout relatively low sea-level episodes (RRI 1985; EGPC 1992). Abu Roash Formation is distinguished by a repeated alternation of deltaic, coastal and shallow marine facies (Hewaidy et al. 2018).

Abu Roash C Member at AG Basin is mainly composed of sandstone, shale and siltstone beds with few limestone streaks. It was deposited in shallow marine shelf (Labib 1985) as part of a major transgression started in the Cenomanian and completed in the Maastrichtian age (EGPC 1992). The sandstone of Abu Roash C Member at Badr El Din-15 Field within AG Basin displays good oil-reservoir properties (Barakat and Nooh 2017).

However, Abu Roash E Member was deposited in a variety of depositional environments including supra-tidal, tidal flats, tidal channels, carbonate inner ramp and tide-dominated deltaic facies (Hewaidy et al. 2018). The sandstones of Abu

Fig. 2 Lithostratigraphic column of Abu Gharadig Field (After El Gazzar et al. 2016)

Era	Period	Epoch	Lithology	Formation	Average Thickness (m)	Mega-sequences	Petroleum Habitat
CENOZOIC	Tertiary	Miocene		Moghra	600	Late Syn-inversion	
		Oligocene		Dabaa	600		
		Eocene L/M/E, Paleocene		Apollonia	700	Syn-inversion	
MESOZOIC	Cretaceous	Campanian Maastrichtian		Khoman	800		
		Santonian					
		Coniacian		Abu Roash	500	Syn-rift	
		Turonian					
		Cenomanian		Bahariya	300+		
		Albian		Kharita	Not penetrated		
		Aptian		Alamein	Not penetrated		
		Barremian - Neocomian		Alam El Bueib	Not penetrated		
	Jurassic	Late		Masajid	Not penetrated		
		Middle		Khatatba	Not penetrated		
		Early		Ras Qattara	Not penetrated		

Sandstone, Dolomite, Limestone, Chalk, Shale

S=Source R=Reservoir C=Seal

Roash "E" Member are also a hydrocarbon-producing horizon in Abu Gharadig Field with AG Basin (Hewaidy et al. 2018).

Data and methods

Seventeen seismic sections cover Abu Gharadig Field have been interpreted using Petrel software. These seismic data contain twelve crosslines of 25 km length and five inline sections extend for 55 km distance. The seismic profiles were tied to two drilled wells, Abu Gharadig-6 (AG-6) and Abu Gharadig-15 (AG-15), as displayed in Fig. 3.

The traditional wireline logs for AG-6 and AG-15 wells are also obtainable and have been analysed using Techlog software. These well-log data consist of CALI "Caliper", BS "Bit Size", DRHO "Density Correction", GR "Gamma Ray", DT "Sonic", RS "Shallow Resistivity", RD "Deep Resistivity", RM "Medium Resistivity", RHOB "Density", NPHI "Neutron" logs as shown in Figs. 4 and 5. The formation evaluation logs for AG-6 and AG-15 wells and the composite log for AG-6 Well are also available in the present study.

The applied methods in this study started with picking the seismic reflector corresponding to the topmost of Abu Roash D Member over the grid of seismic lines as well as the related faults (Figs. 6 and 7). The reason of choosing the seismic horizon of the top of Abu Roash D Member rather than Abu Roash C or E members to be picked on seismic data is due to the seismic reflectors corresponding to both members, which are not noticeable enough to be traced on the seismic profiles according to the low contrast in the acoustic impedance. However, the reflector of Abu Roash D Member is clear and obvious over the whole seismic grid since it displays high contrast between its entire lithology

Fig. 3 Seismic lines and location of the AG-6 and AG-15 wells within Abu Gharadig Field
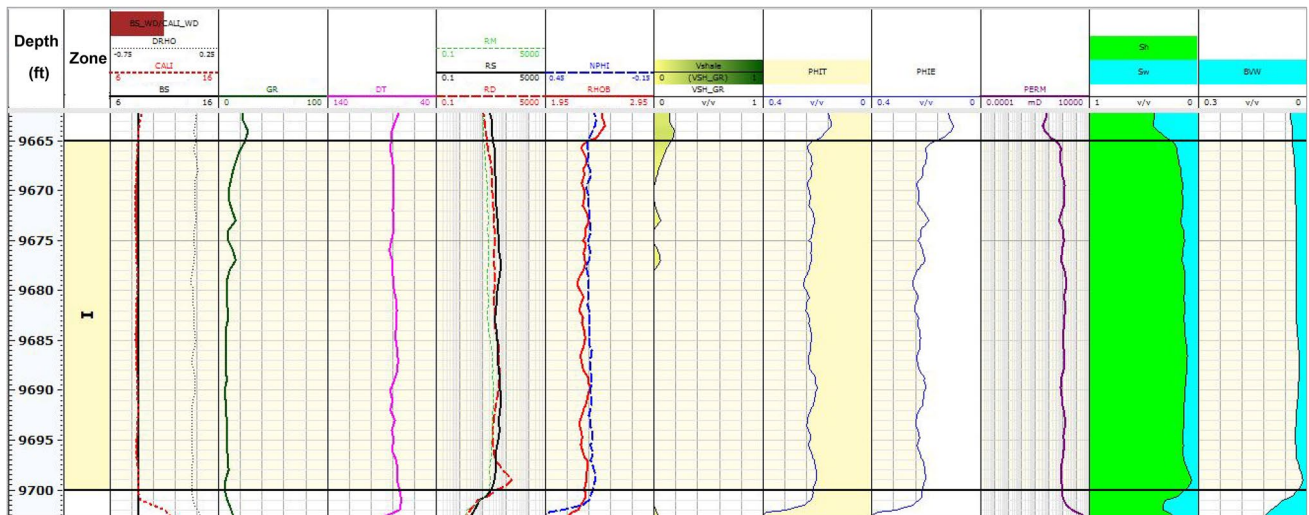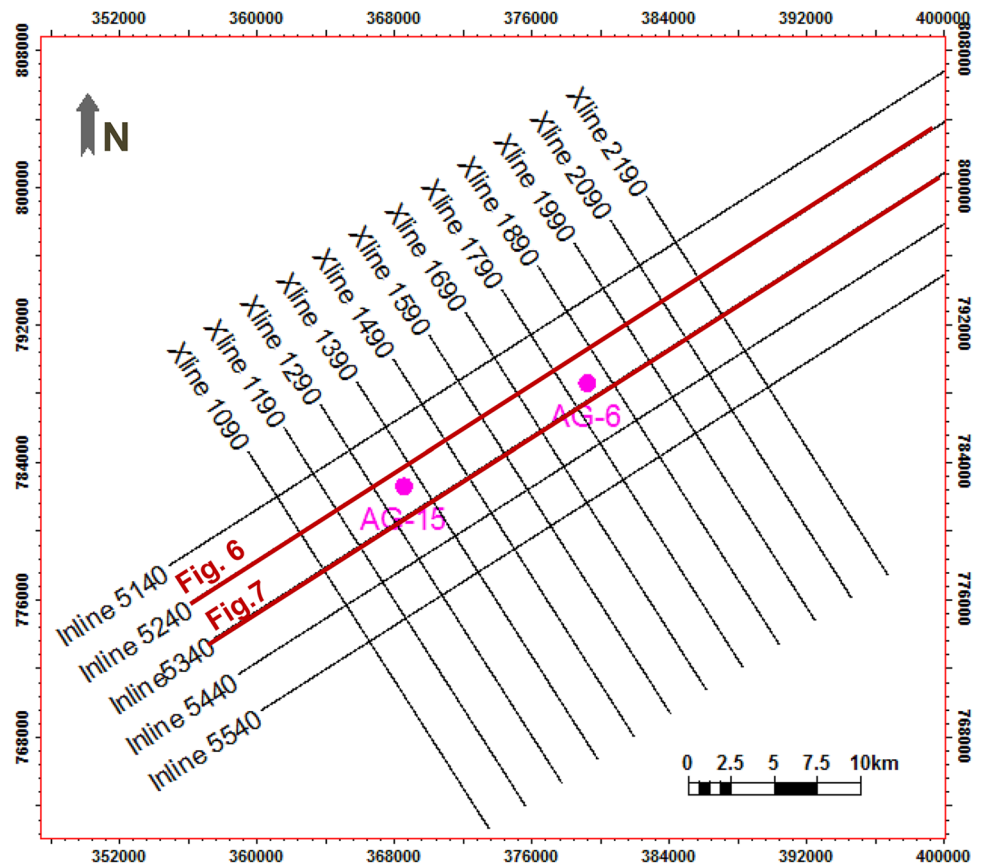
Fig. 4 Wireline log suite with interpretation for zone I in AG-6 Well

(limestone) and the overlying clastics of Abu Roash C Member as shown in Figs. 6 and 7.

The picked horizon of Abu Roash D Member with the accompanying faults was mapped in depth unit (Fig. 8), and the mapped structures were examined in terms of the tectonic background of AG Basin in the Late Cretaceous time.

The previous step has been followed by qualitative and quantitative investigation for the wireline logs data of the studied wells to distinguish the possible hydrocarbon-bearing zones within Abu Roash C and E members in Abu Gharadig Field.
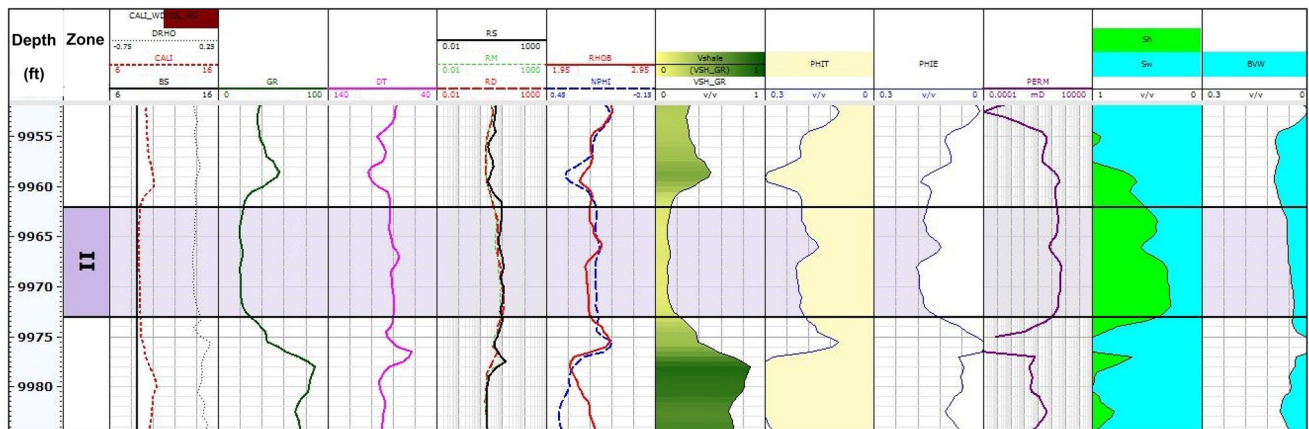
Fig. 5 Wireline log suite with interpretation for zone II in AG-15Well
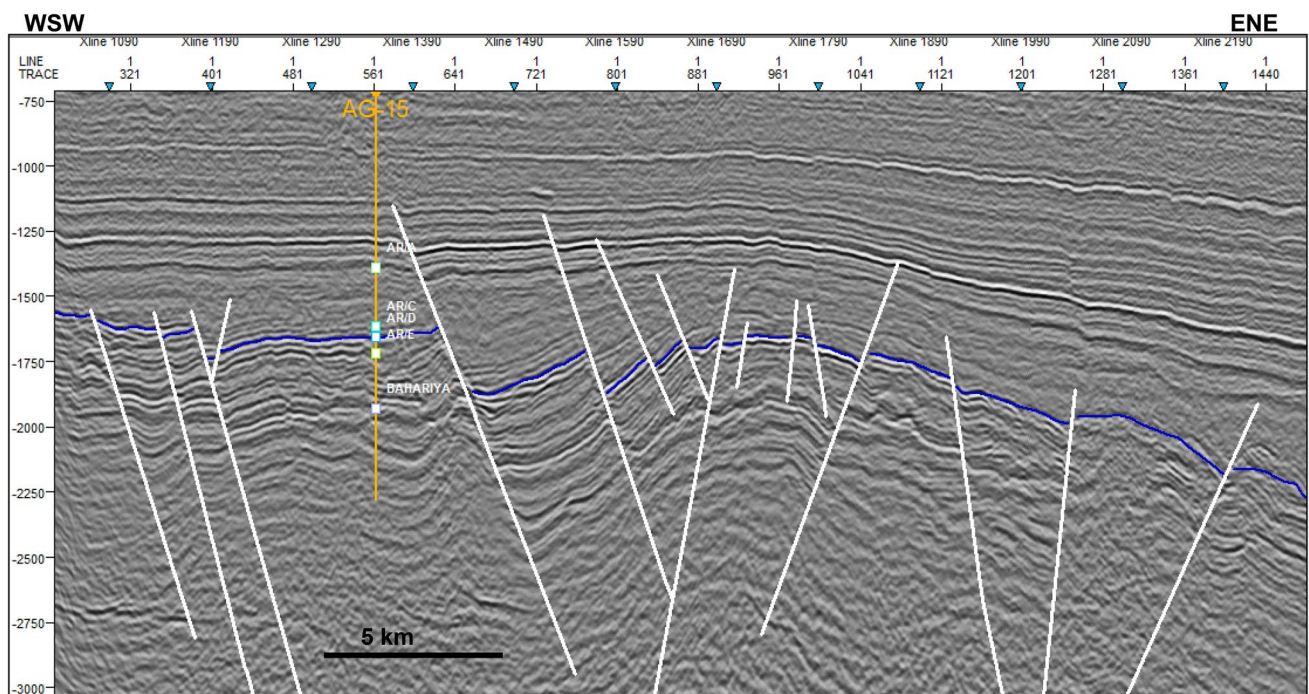

Fig. 6 Interpreted seismic line No. 5240 (see Fig. 3 for line location)

This step revealed that the optimistic zones within AG-6 Well locate within Abu Roash "C" Member between depths 9665–9700 ft (zone I). However, the appreciative zone in AG-15 occurs in Abu Roash "E" Member between depths 9962–9973 ft (zone II).

The qualitative evaluation of the wireline logs revealed that zone I and zone II are the only zones displaying positive criteria to be potential hydrocarbon reservoirs. These criteria encompass the gamma-ray log displays fairly consistent low values, which approves the clean nature (i.e. low-shale content) of the examined sandy intervals, the presence of

crossover feature between neutron and density logs characterising the sandstone matrix (i.e. deflection of neutron curve to right and the density log to the left), the relatively high deep resistivity values which confirms the existence of the non-conducive hydrocarbon and the calliper curve shows mudcake opposite the examined intervals.

Consequently, the suites of wireline logs for the motivating zones (I and II) have been quantifiable assessed. This evaluation involves the calculations of the essential petrophysical parameters required for appraising the quality of hydrocarbon reservoirs. These calculations include shale volume; total
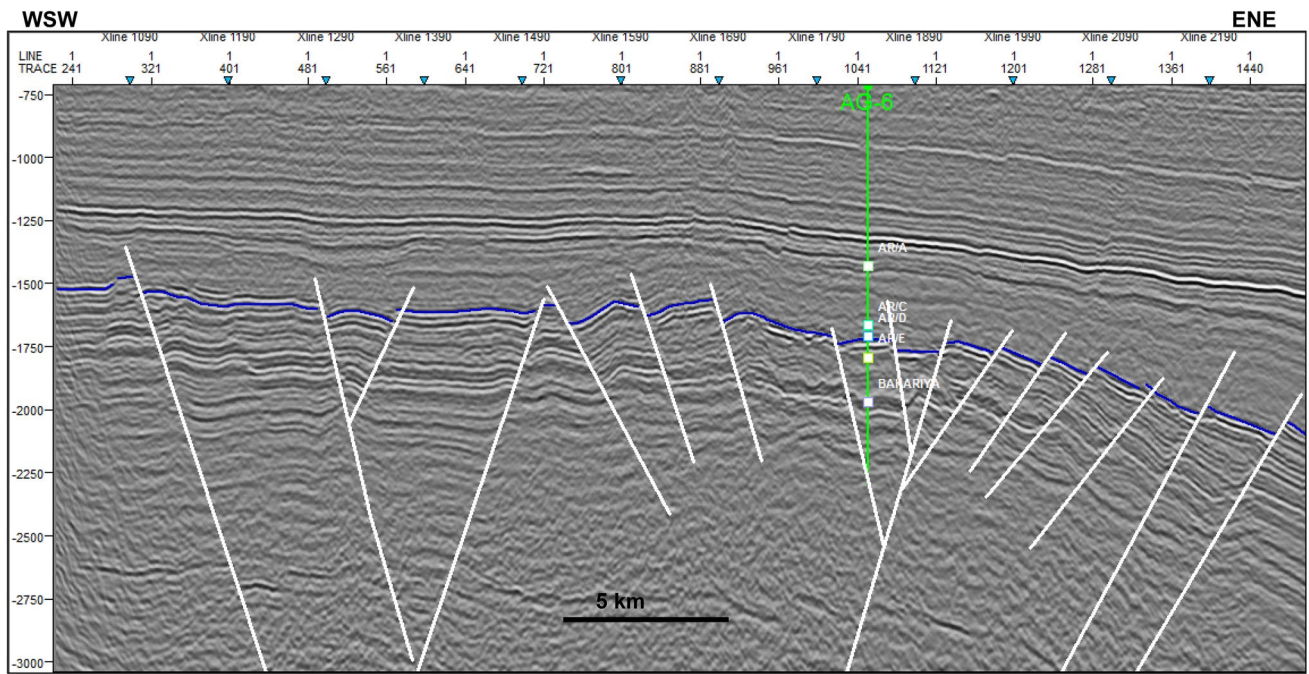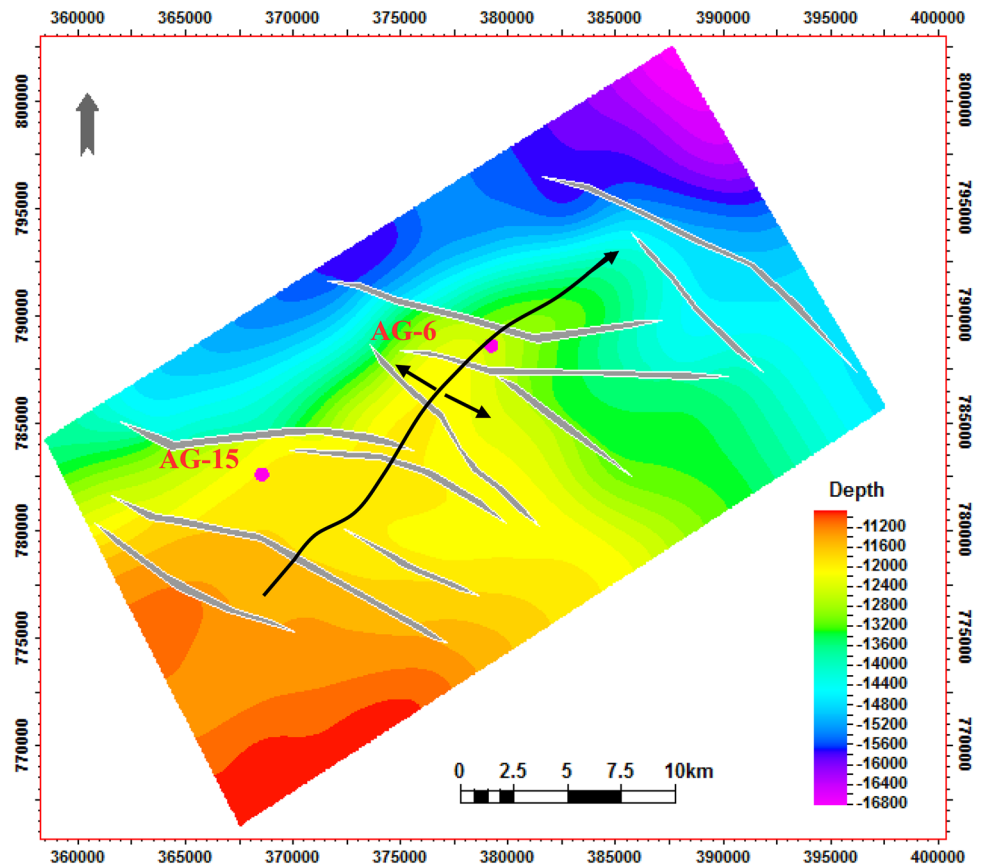
Fig. 7 Interpreted seismic line No. 5340 (see Fig. 3 for line location)

Fig. 8 Depth-structure map for the topmost surface of Abu Roash D Member in the study area. Note the presence of the ENE–WSW asymmetrical anticline which plunges to NE and its fragmentation by abundant NW–SE extensional faults

porosity; effective porosity; water saturation; bulk volume of water; absolute permeability; and irreducible water saturation. The obtained results of these parameters are displayed in Tables 1 and 2 for zones I and II, respectively.

Results

Seismic data interpretation

The seismic reflector corresponds to the top of Abu Roash D Member exhibiting strong amplitude that intersected by numerous normal faults (Figs. 6 and 7). The structure map for the examined surface displays asymmetrical anticline strikes ENE–WSW and plunges to NE (Fig. 8). This anticlinal fold fragmented by abundant NW–SE extensional faults varies in length between 5 and 12 km (Fig. 8). The association of the interpreted anticline, which represents the compressional structure plus the investigated normal faults which reflect the extensional regime, is a strong evidence for the dextral wrench tectonic affected AG Basin. This dextral wrench resulted by the NW motion of African Plate is compared to the Laurasia Plate in the Late Cretaceous episode.

Well-log appraisal

The visual examination of the created neutron density plots (Schlumberger 1972) for the examined zones shows the clustering of the plotted points on and around the sandstone line reflecting the sandy matrix of zones I and II as shown in Fig. 9. Moreover, water saturation-effective porosity plots (Asquith and Gibson 1982) have been constructed to judge the grain size for the interesting zones as displayed in Fig. 10. These plots display that the sand grains for zone I are coarse-grained, whereas the sand grains for zone II are fine- to medium-grained in size.

Shale volume (Vsh)

The clay amount in the examined zones as displayed in track six in Figs. 4 and 5 has been determined depending on the gamma-ray log in a linear response using the following equation (Asquith and Gibson 1982):

$$V_{sh} = \frac{\left(GR - GR_{min}\right)}{\left(GR_{max} - GR_{min}\right)} \tag{1}$$

where V_{sh} shale volume; GR gamma-ray reading value; GR_{min} the lowest gamma-ray value; GR_{max} the maximum gamma-ray value.

The calculated V_{sh} in zone I is quite very low (0.01), while the shale volume value increases in zone II and reaches 0.13.

Total porosity (ϕT)

Total porosity has been calculated from the neutron-density logs and is presented in track seven in Figs. 4 and 5 using the following formula (Asquith and Gibson 1982):

$$\phi_T = \frac{\phi_N + \phi_D}{2} \tag{2}$$

where ϕ_T the total porosity; ϕ_N the neutron porosity; ϕ_D the density porosity.

The average total porosity is high in both zones. It reaches 22% in zone I and 20% in zone II.

Effective porosity (ϕe)

The effective porosity as displayed in track eight in Figs. 4 and 5 has been determined by the next equation (after Asquith and Gibson 1982):

$$\phi_e = \phi_T * \left(1 - V_{sh}\right) \tag{3}$$

where ϕ_e the effective porosity; ϕ_T the total porosity; V_{sh} the shale volume.

The average effective porosity is high in both zones. It reaches 22% in zone I and 16% in zone II. This variation is due to the higher amount of shale in zone II rather than zone I.

Absolute permeability

The absolute permeability for the examined zones has been determined and is shown in track nine in Figs. 4 and 5 using Wyllie and Rose equation (Wyllie and Rose 1950).

The determined values of absolute permeability were high in zone I (113 mD), whereas in zone II was only (27 mD). This difference is due to the low amount of shale plus the presence of coarse-grained sands zone I; however, the sand grains for zone II are smaller (fine- to medium-grained), and also it has higher amount of shale in zone II rather than zone I.

Water saturation (Sw)

Water saturation for the interesting zones has been computed by the Indonesia model (Poupon and Leveaux 1971):

Table 1 Well-log data and output results for zone I in AG-6 Well

	Input well-log data											Output results							
Depth (ft)	Bit size (IN)	Calliper (IN)	Density correction (G/C3)	Gamma ray (API)	Sonic (US/F)	Shallow resistivity (Ωm2/m)	Medium resistivity (Ωm2/m)	Deep resistivity (Ωm2/m)	Neutron porosity	Density (G/C3)		CALI-BS (IN)	Shale volume	Total porosity	Effective porosity	K (mD)	Water saturation	Bulk volume of water	Irreducible water saturation
9665	8.63	8.57	0.04	24.53	81.67	26.93	10.90	15.16	0.22	2.34		−0.05	0.16	0.22	0.17	33.78	0.24	0.04	0.13
9665.25	8.63	8.56	0.04	23.21	81.77	28.62	11.21	15.63	0.22	2.32		−0.07	0.15	0.23	0.18	47.54	0.22	0.04	0.12
9665.5	8.63	8.55	0.03	21.89	81.87	30.31	11.52	16.09	0.22	2.29		−0.08	0.13	0.24	0.20	66.05	0.21	0.04	0.11
9665.75	8.63	8.53	0.03	20.57	81.97	32.00	11.83	16.56	0.22	2.28		−0.09	0.12	0.24	0.20	75.66	0.20	0.04	0.11
9666	8.63	8.52	0.02	19.25	82.07	33.68	12.14	17.02	0.21	2.29		−0.11	0.10	0.23	0.20	74.56	0.20	0.04	0.11
9666.25	8.63	8.51	0.03	18.44	81.59	33.22	12.42	18.21	0.21	2.30		−0.12	0.09	0.23	0.20	71.79	0.19	0.04	0.11
9666.5	8.63	8.50	0.04	17.63	81.11	32.76	12.71	19.40	0.21	2.32		−0.13	0.08	0.22	0.20	68.50	0.19	0.04	0.11
9666.75	8.63	8.48	0.05	16.82	80.63	32.29	12.99	20.59	0.21	2.33		−0.14	0.08	0.22	0.20	68.19	0.19	0.04	0.11
9667	8.63	8.47	0.05	16.01	80.15	31.83	13.27	21.78	0.22	2.33		−0.15	0.07	0.22	0.20	73.07	0.18	0.04	0.11
9667.25	8.63	8.46	0.05	15.30	80.02	32.25	13.41	22.43	0.22	2.33		−0.16	0.06	0.22	0.20	74.08	0.18	0.04	0.11
9667.5	8.63	8.46	0.05	14.59	79.89	32.66	13.55	23.07	0.21	2.32		−0.17	0.05	0.22	0.21	85.36	0.17	0.04	0.11
9667.75	8.63	8.45	0.06	13.88	79.75	33.08	13.69	23.72	0.21	2.30		−0.18	0.04	0.23	0.21	94.40	0.16	0.03	0.10
9668	8.63	8.44	0.06	13.17	79.62	33.50	13.82	24.37	0.20	2.31		−0.19	0.04	0.22	0.21	93.56	0.16	0.03	0.11
9668.25	8.63	8.43	0.05	12.66	79.63	34.19	14.16	24.52	0.20	2.31		−0.20	0.03	0.22	0.21	95.32	0.16	0.03	0.10
9668.5	8.63	8.42	0.05	12.16	79.65	34.88	14.49	24.67	0.20	2.31		−0.21	0.02	0.22	0.21	97.10	0.16	0.03	0.10
9668.75	8.63	8.41	0.04	11.65	79.66	35.57	14.82	24.82	0.20	2.30		−0.22	0.02	0.23	0.22	112.01	0.16	0.03	0.10
9669	8.63	8.40	0.03	11.15	79.67	36.26	15.15	24.97	0.21	2.29		−0.23	0.01	0.23	0.23	127.77	0.15	0.03	0.10
9669.25	8.63	8.39	0.03	10.64	79.52	36.58	15.27	25.08	0.22	2.29		−0.23	0.01	0.24	0.23	143.87	0.15	0.03	0.10
9669.5	8.63	8.38	0.03	10.13	79.37	36.91	15.40	25.20	0.22	2.29		−0.24	0.00	0.24	0.24	145.43	0.15	0.03	0.10
9669.75	8.63	8.37	0.03	9.63	79.21	37.23	15.52	25.31	0.22	2.30		−0.26	0.00	0.23	0.23	138.39	0.15	0.03	0.10
9670	8.63	8.36	0.03	9.12	79.06	37.55	15.64	25.42	0.22	2.31		−0.27	0.00	0.23	0.23	129.59	0.15	0.03	0.10
9670.25	8.63	8.36	0.03	9.22	79.16	37.38	15.50	26.06	0.22	2.31		−0.27	0.00	0.23	0.23	126.62	0.15	0.03	0.10
9670.5	8.63	8.36	0.03	9.32	79.27	37.20	15.36	26.69	0.21	2.31		−0.27	0.00	0.23	0.23	122.79	0.15	0.03	0.10
9670.75	8.63	8.36	0.03	9.42	79.37	37.03	15.22	27.33	0.21	2.31		−0.27	0.00	0.23	0.23	124.03	0.15	0.03	0.10
9671	8.63	8.36	0.03	9.53	79.47	36.85	15.07	27.97	0.21	2.30		−0.27	0.00	0.23	0.23	129.79	0.14	0.03	0.10
9671.25	8.63	8.36	0.03	10.23	79.62	37.57	15.46	28.23	0.21	2.30		−0.26	0.01	0.23	0.23	130.49	0.14	0.03	0.10
9671.5	8.63	8.37	0.03	10.94	79.76	38.29	15.85	28.49	0.21	2.30		−0.26	0.02	0.23	0.23	128.19	0.14	0.03	0.10
9671.75	8.63	8.37	0.04	11.65	79.91	39.00	16.23	28.75	0.21	2.31		−0.26	0.03	0.23	0.22	108.99	0.15	0.03	0.10
9672	8.63	8.37	0.04	12.36	80.05	39.72	16.62	29.02	0.20	2.32		−0.26	0.04	0.22	0.21	92.11	0.15	0.03	0.11
9672.25	8.63	8.37	0.04	13.17	79.88	40.58	16.80	29.02	0.21	2.33		−0.25	0.04	0.22	0.21	80.26	0.15	0.03	0.11
9672.5	8.63	8.38	0.04	13.98	79.72	41.44	16.97	29.03	0.21	2.34		−0.25	0.04	0.21	0.20	72.50	0.16	0.03	0.11
9672.75	8.63	8.38	0.04	14.79	79.55	42.30	17.15	29.04	0.21	2.34		−0.25	0.05	0.21	0.20	64.36	0.16	0.03	0.11
9673	8.63	8.38	0.04	15.60	79.38	43.15	17.32	29.04	0.21	2.35		−0.24	0.06	0.21	0.19	58.42	0.16	0.03	0.12
9673.25	8.63	8.38	0.04	13.88	79.35	43.63	17.03	29.88	0.20	2.35		−0.24	0.04	0.21	0.20	66.52	0.16	0.03	0.11

Table 1 (continued)

	Input well-log data											Output results							
Depth (ft)	Bit size (IN)	Calliper (IN)	Density correction (G/C3)	Gamma ray (API)	Sonic (US/F)	Shallow resistivity (Ωm2/m)	Medium resistivity (Ωm2/m)	Deep resistivity (Ωm2/m)	Neutron porosity	Density (G/C3)		CALI-BS (IN)	Shale volume	Total porosity	Effective porosity	K (mD)	Water saturation	Bulk volume of water	Irreducible water saturation
9673.5	8.63	8.39	0.03	12.16	79.33	44.11	16.74	30.72	0.20	2.33		−0.24	0.02	0.21	0.21	81.07	0.15	0.03	0.11
9673.75	8.63	8.39	0.03	10.44	79.30	44.59	16.44	31.55	0.20	2.32		−0.24	0.00	0.22	0.22	99.15	0.14	0.03	0.10
9674	8.63	8.39	0.02	8.72	79.27	45.06	16.15	32.39	0.20	2.32		−0.23	0.00	0.22	0.22	108.05	0.14	0.03	0.10
9674.25	8.63	8.39	0.02	8.72	79.76	46.35	16.55	32.49	0.20	2.32		−0.23	0.00	0.22	0.22	108.86	0.14	0.03	0.10
9674.5	8.63	8.40	0.02	8.72	80.25	47.63	16.95	32.59	0.20	2.32		−0.23	0.00	0.22	0.22	109.67	0.14	0.03	0.10
9674.75	8.63	8.40	0.02	8.72	80.73	48.91	17.35	32.70	0.21	2.31		−0.23	0.00	0.22	0.22	115.83	0.14	0.03	0.10
9675	8.63	8.40	0.02	8.72	81.22	50.19	17.75	32.80	0.21	2.29		−0.23	0.00	0.23	0.23	138.26	0.13	0.03	0.10
9675.25	8.63	8.41	0.02	9.83	81.69	50.10	17.83	32.33	0.21	2.32		−0.22	0.00	0.22	0.22	116.66	0.14	0.03	0.10
9675.5	8.63	8.42	0.03	10.94	82.15	50.01	17.91	31.86	0.21	2.32		−0.21	0.01	0.22	0.22	108.33	0.14	0.03	0.10
9675.75	8.63	8.42	0.03	12.06	82.62	49.92	17.99	31.39	0.21	2.32		−0.20	0.02	0.22	0.21	98.18	0.14	0.03	0.11
9676	8.63	8.43	0.03	13.17	83.08	49.82	18.07	30.92	0.20	2.31		−0.20	0.04	0.22	0.21	92.96	0.14	0.03	0.11
9676.25	8.63	8.44	0.03	13.78	82.45	51.89	18.07	30.66	0.20	2.30		−0.19	0.04	0.23	0.21	93.62	0.14	0.03	0.11
9676.5	8.63	8.45	0.03	14.39	81.82	53.97	18.07	30.41	0.20	2.31		−0.18	0.05	0.22	0.21	86.50	0.15	0.03	0.11
9676.75	8.63	8.46	0.03	14.99	81.19	56.04	18.07	30.15	0.21	2.31		−0.16	0.06	0.22	0.21	81.74	0.15	0.03	0.11
9677	8.63	8.47	0.03	15.60	80.56	58.11	18.06	29.90	0.21	2.31		−0.15	0.06	0.22	0.20	79.08	0.15	0.03	0.11
9677.25	8.63	8.48	0.02	14.18	80.44	57.90	17.62	30.61	0.22	2.32		−0.15	0.05	0.22	0.21	90.29	0.15	0.03	0.11
9677.5	8.63	8.49	0.02	12.77	80.32	57.70	17.18	31.32	0.22	2.31		−0.14	0.03	0.23	0.22	107.40	0.14	0.03	0.10
9677.75	8.63	8.50	0.01	11.35	80.19	57.49	16.73	32.04	0.22	2.31		−0.13	0.01	0.23	0.23	120.07	0.14	0.03	0.10
9678	8.63	8.51	0.01	9.93	80.07	57.28	16.29	32.75	0.22	2.30		−0.12	0.00	0.23	0.23	142.07	0.13	0.03	0.10
9678.25	8.63	8.51	0.01	9.32	80.02	55.23	16.32	32.72	0.22	2.28		−0.11	0.00	0.24	0.24	152.31	0.13	0.03	0.09
9678.5	8.63	8.52	0.00	8.72	79.97	53.18	16.35	32.69	0.21	2.27		−0.11	0.00	0.24	0.24	163.19	0.13	0.03	0.09
9678.75	8.63	8.52	0.00	8.11	79.92	51.12	16.39	32.66	0.21	2.26		−0.11	0.00	0.25	0.25	176.38	0.12	0.03	0.09
9679	8.63	8.52	−0.01	7.50	79.87	49.07	16.42	32.63	0.21	2.25		−0.11	0.00	0.25	0.25	182.74	0.12	0.03	0.09
9679.25	8.63	8.52	0.00	7.50	79.61	47.42	16.39	32.36	0.21	2.25		−0.11	0.00	0.25	0.25	191.56	0.12	0.03	0.09
9679.5	8.63	8.51	0.00	7.50	79.34	45.77	16.35	32.09	0.21	2.25		−0.12	0.00	0.25	0.25	189.05	0.12	0.03	0.09
9679.75	8.63	8.51	0.01	7.50	79.08	44.12	16.32	31.82	0.21	2.26		−0.12	0.00	0.25	0.25	176.27	0.13	0.03	0.09
9680	8.63	8.50	0.02	7.50	78.81	42.46	16.29	31.55	0.22	2.27		−0.13	0.00	0.24	0.24	164.24	0.13	0.03	0.09
9680.25	8.63	8.49	0.02	7.50	78.32	41.92	16.55	31.49	0.21	2.28		−0.13	0.00	0.24	0.24	149.43	0.13	0.03	0.09
9680.5	8.63	8.49	0.01	7.50	77.84	41.37	16.81	31.43	0.21	2.30		−0.14	0.00	0.23	0.23	135.82	0.13	0.03	0.10
9680.75	8.63	8.48	0.01	7.50	77.35	40.82	17.07	31.37	0.21	2.30		−0.15	0.00	0.23	0.23	134.06	0.13	0.03	0.10
9681	8.63	8.47	0.01	7.50	76.86	40.27	17.33	31.31	0.22	2.29		−0.15	0.00	0.23	0.23	145.25	0.13	0.03	0.10
9681.25	8.63	8.47	0.01	7.70	76.71	39.35	17.11	31.51	0.22	2.28		−0.16	0.00	0.24	0.24	155.92	0.13	0.03	0.09

Table 1 (continued)

	Input well-log data											Output results							
Depth (ft)	Bit size (IN)	Calliper (IN)	Density correction (G/C3)	Gamma ray (API)	Sonic (US/F)	Shallow resistivity (Ωm2/m)	Medium resistivity (Ωm2/m)	Deep resistivity (Ωm2/m)	Neutron porosity	Density (G/C3)		CALI-BS (IN)	Shale volume	Total porosity	Effective porosity	K (mD)	Water saturation	Bulk volume of water	Irreducible water saturation
9681.5	8.63	8.46	0.02	7.91	76.57	38.44	16.89	31.71	0.22	2.27		−0.16	0.00	0.24	0.24	161.66	0.13	0.03	0.09
9681.75	8.63	8.46	0.02	8.11	76.42	37.52	16.67	31.91	0.21	2.27		−0.17	0.00	0.24	0.24	164.41	0.13	0.03	0.09
9682	8.63	8.45	0.02	8.31	76.27	36.60	16.45	32.11	0.21	2.26		−0.18	0.00	0.24	0.24	165.96	0.13	0.03	0.09
9682.25	8.63	8.44	0.02	8.31	76.45	35.79	16.53	32.25	0.21	2.28		−0.18	0.00	0.24	0.24	150.95	0.13	0.03	0.09
9682.5	8.63	8.44	0.02	8.31	76.62	34.98	16.60	32.40	0.20	2.29		−0.19	0.00	0.23	0.23	135.99	0.13	0.03	0.10
9682.75	8.63	8.43	0.02	8.31	76.80	34.17	16.68	32.55	0.20	2.30		−0.20	0.00	0.23	0.23	127.43	0.13	0.03	0.10
9683	8.63	8.42	0.02	8.31	76.97	33.36	16.75	32.69	0.20	2.29		−0.21	0.00	0.23	0.23	132.13	0.13	0.03	0.10
9683.25	8.63	8.41	0.02	7.80	77.05	34.81	17.14	33.30	0.21	2.29		−0.21	0.00	0.23	0.23	138.61	0.13	0.03	0.10
9683.5	8.63	8.41	0.03	7.30	77.12	36.25	17.54	33.92	0.21	2.29		−0.22	0.00	0.23	0.23	133.31	0.13	0.03	0.10
9683.75	8.63	8.40	0.03	6.79	77.20	37.70	17.93	34.53	0.21	2.30		−0.23	0.00	0.23	0.23	125.47	0.13	0.03	0.10
9684	8.63	8.39	0.03	6.29	77.27	39.14	18.32	35.14	0.21	2.31		−0.23	0.00	0.22	0.22	117.92	0.13	0.03	0.10
9684.25	8.63	8.39	0.03	6.39	77.27	39.98	19.12	37.30	0.21	2.31		−0.24	0.00	0.22	0.22	115.00	0.13	0.03	0.10
9684.5	8.63	8.39	0.03	6.49	77.27	40.81	19.92	39.46	0.21	2.31		−0.24	0.00	0.22	0.22	113.73	0.12	0.03	0.10
9684.75	8.63	8.38	0.04	6.59	77.27	41.65	20.72	41.62	0.21	2.32		−0.24	0.00	0.22	0.22	110.90	0.12	0.03	0.10
9685	8.63	8.38	0.04	6.69	77.27	42.48	21.52	43.78	0.21	2.31		−0.24	0.00	0.22	0.22	113.90	0.12	0.03	0.10
9685.25	8.63	8.39	0.03	6.59	76.93	42.88	22.24	45.73	0.21	2.31		−0.24	0.00	0.22	0.22	117.06	0.11	0.03	0.10
9685.5	8.63	8.40	0.03	6.49	76.59	43.27	22.96	47.67	0.20	2.31		−0.23	0.00	0.23	0.23	120.20	0.11	0.03	0.10
9685.75	8.63	8.40	0.02	6.39	76.25	43.67	23.68	49.62	0.20	2.30		−0.22	0.00	0.23	0.23	121.23	0.11	0.02	0.10
9686	8.63	8.41	0.02	6.29	75.91	44.06	24.40	51.57	0.19	2.29		−0.22	0.00	0.23	0.23	124.10	0.11	0.02	0.10
9686.25	8.63	8.42	0.01	6.49	75.74	44.08	24.88	51.43	0.19	2.28		−0.21	0.00	0.23	0.23	133.28	0.10	0.02	0.10
9686.5	8.63	8.43	0.01	6.69	75.58	44.11	25.36	51.28	0.20	2.27		−0.20	0.00	0.23	0.23	142.99	0.10	0.02	0.10
9686.75	8.63	8.43	0.01	6.89	75.41	44.13	25.84	51.13	0.20	2.28		−0.19	0.00	0.23	0.23	141.89	0.10	0.02	0.10
9687	8.63	8.44	0.00	7.10	75.24	44.16	26.32	50.98	0.20	2.28		−0.19	0.00	0.23	0.23	140.91	0.10	0.02	0.10
9687.25	8.63	8.45	0.01	6.99	75.38	45.40	26.60	51.25	0.20	2.29		−0.18	0.00	0.23	0.23	137.40	0.10	0.02	0.10
9687.5	8.63	8.46	0.01	6.89	75.52	46.65	26.88	51.52	0.20	2.29		−0.17	0.00	0.23	0.23	133.01	0.10	0.02	0.10
9687.75	8.63	8.46	0.02	6.79	75.65	47.89	27.16	51.78	0.20	2.29		−0.16	0.00	0.23	0.23	127.38	0.11	0.02	0.10
9688	8.63	8.47	0.02	6.69	75.79	49.14	27.44	52.05	0.20	2.30		−0.15	0.00	0.23	0.23	120.16	0.11	0.02	0.10
9688.25	8.63	8.48	0.03	6.89	76.52	50.81	27.31	51.93	0.20	2.32		−0.15	0.00	0.22	0.22	105.65	0.11	0.02	0.10
9688.5	8.63	8.49	0.03	7.10	77.25	52.48	27.19	51.80	0.20	2.33		−0.14	0.00	0.21	0.21	92.60	0.11	0.02	0.11
9688.75	8.63	8.49	0.03	7.30	77.98	54.15	27.06	51.68	0.20	2.35		−0.13	0.00	0.21	0.21	81.37	0.12	0.02	0.11
9689	8.63	8.50	0.03	7.50	78.71	55.83	26.93	51.55	0.20	2.34		−0.13	0.00	0.21	0.21	84.89	0.12	0.02	0.11
9689.25	8.63	8.51	0.03	6.99	79.61	56.07	27.60	50.42	0.20	2.35		−0.12	0.00	0.21	0.21	81.11	0.12	0.02	0.11

Table 1 (continued)

	Input well-log data										Output results							
Depth (ft)	Bit size (IN)	Calliper (IN)	Density correction (G/C3)	Gamma ray (API)	Sonic (US/F)	Shallow resistivity (Ωm2/m)	Medium resistivity (Ωm2/m)	Deep resistivity (Ωm2/m)	Neutron porosity	Density (G/C3)	CALI-BS (IN)	Shale volume	Total porosity	Effective porosity	K (mD)	Water saturation	Bulk volume of water	Irreducible water saturation
9689.5	8.63	8.52	0.03	6.49	80.52	56.30	28.28	49.29	0.20	2.35	−0.11	0.00	0.20	0.20	77.48	0.12	0.02	0.11
9689.75	8.63	8.53	0.03	5.98	81.42	56.54	28.95	48.16	0.20	2.37	−0.10	0.00	0.20	0.20	72.57	0.12	0.02	0.11
9690	8.63	8.54	0.04	5.48	82.32	56.78	29.62	47.04	0.20	2.36	−0.09	0.00	0.21	0.21	80.71	0.12	0.03	0.11
9690.25	8.63	8.55	0.03	5.68	81.83	57.60	29.72	45.29	0.20	2.35	−0.08	0.00	0.21	0.21	84.68	0.12	0.03	0.11
9690.5	8.63	8.56	0.02	5.88	81.35	58.41	29.81	43.55	0.20	2.34	−0.07	0.00	0.21	0.21	86.11	0.13	0.03	0.11
9690.75	8.63	8.56	0.02	6.08	80.86	59.23	29.90	41.81	0.20	2.34	−0.06	0.00	0.21	0.21	89.59	0.13	0.03	0.11
9691	8.63	8.57	0.01	6.29	80.37	60.04	29.99	40.07	0.20	2.33	−0.05	0.00	0.21	0.21	93.18	0.13	0.03	0.11
9691.25	8.63	8.58	0.01	6.29	80.81	59.04	29.18	38.46	0.20	2.33	−0.05	0.00	0.21	0.21	95.34	0.13	0.03	0.10
9691.5	8.63	8.59	0.01	6.29	81.25	58.05	28.37	36.84	0.19	2.32	−0.04	0.00	0.21	0.21	97.47	0.13	0.03	0.10
9691.75	8.63	8.59	0.01	6.29	81.69	57.05	27.56	35.22	0.20	2.31	−0.03	0.00	0.22	0.22	112.59	0.13	0.03	0.10
9692	8.63	8.60	0.01	6.29	82.13	56.06	26.74	33.61	0.20	2.30	−0.03	0.00	0.23	0.23	122.09	0.13	0.03	0.10
9692.25	8.63	8.59	0.01	6.59	81.10	54.16	26.43	32.57	0.21	2.29	−0.04	0.00	0.23	0.23	131.35	0.13	0.03	0.10
9692.5	8.63	8.58	0.00	6.89	80.08	52.27	26.12	31.53	0.21	2.29	−0.04	0.00	0.23	0.23	142.13	0.13	0.03	0.10
9692.75	8.63	8.57	0.00	7.20	79.05	50.38	25.81	30.50	0.21	2.28	−0.05	0.00	0.24	0.24	146.97	0.13	0.03	0.09
9693	8.63	8.56	0.00	7.50	78.02	48.49	25.49	29.46	0.20	2.27	−0.06	0.00	0.24	0.24	150.91	0.14	0.03	0.09
9693.25	8.63	8.55	0.00	7.50	78.76	49.71	25.97	28.97	0.20	2.27	−0.08	0.00	0.24	0.24	153.90	0.14	0.03	0.09
9693.5	8.63	8.54	0.00	7.50	79.51	50.94	26.44	28.48	0.20	2.27	−0.09	0.00	0.24	0.24	155.83	0.14	0.03	0.09
9693.75	8.63	8.52	0.00	7.50	80.25	52.16	26.91	27.99	0.20	2.27	−0.10	0.00	0.24	0.24	146.57	0.14	0.03	0.09
9694	8.63	8.51	0.01	7.50	80.99	53.39	27.38	27.49	0.19	2.28	−0.12	0.00	0.23	0.23	135.65	0.14	0.03	0.10
9694.25	8.63	8.50	0.00	7.60	80.55	51.71	26.71	27.48	0.19	2.28	−0.13	0.00	0.23	0.23	126.89	0.14	0.03	0.10
9694.5	8.63	8.49	0.00	7.70	80.10	50.04	26.04	27.46	0.19	2.29	−0.14	0.00	0.23	0.23	122.06	0.15	0.03	0.10
9694.75	8.63	8.47	0.00	7.80	79.66	48.36	25.37	27.45	0.19	2.29	−0.15	0.00	0.22	0.22	119.81	0.15	0.03	0.10
9695	8.63	8.46	0.00	7.91	79.21	46.69	24.70	27.43	0.19	2.29	−0.16	0.00	0.23	0.23	124.78	0.15	0.03	0.10
9695.25	8.63	8.44	0.00	7.91	79.62	44.45	24.43	27.90	0.20	2.28	−0.18	0.00	0.23	0.23	134.82	0.14	0.03	0.10
9695.5	8.63	8.43	0.00	7.91	80.04	42.22	24.16	28.38	0.20	2.28	−0.19	0.00	0.23	0.23	143.38	0.14	0.03	0.10
9695.75	8.63	8.42	0.00	7.91	80.45	39.98	23.90	28.85	0.20	2.28	−0.20	0.00	0.23	0.23	131.90	0.14	0.03	0.10
9696	8.63	8.44	0.00	7.91	80.86	37.74	23.63	29.32	0.19	2.29	−0.21	0.00	0.23	0.23	122.03	0.14	0.03	0.10
9696.25	8.63	8.44	0.01	8.01	79.87	37.09	23.25	30.53	0.19	2.30	−0.19	0.00	0.22	0.22	114.49	0.14	0.03	0.10
9696.5	8.63	8.46	0.01	8.11	78.88	36.44	22.88	31.74	0.19	2.30	−0.16	0.00	0.22	0.22	107.41	0.14	0.03	0.10
9696.75	8.63	8.48	0.01	8.21	77.89	35.79	22.50	32.95	0.19	2.31	−0.15	0.00	0.22	0.22	106.44	0.14	0.03	0.10
9697	8.63	8.50	0.01	8.31	76.90	35.14	22.12	34.15	0.20	2.34	−0.13	0.00	0.21	0.21	92.63	0.14	0.03	0.11
9697.25	8.63	8.52	0.01	8.51	76.59	35.41	21.51	43.14	0.19	2.34	−0.11	0.00	0.21	0.21	88.86	0.13	0.03	0.11

Table 1 (continued)

Input well-log data											Output results							
Depth (ft)	Bit size (IN)	Calliper (IN)	Density correction (G/C3)	Gamma ray (API)	Sonic (US/F)	Shallow resistivity (Ωm2/m)	Medium resistivity (Ωm2/m)	Deep resistivity (Ωm2/m)	Neutron porosity	Density (G/C3)	CALI-BS (IN)	Shale volume	Total porosity	Effective porosity	K (mD)	Water saturation	Bulk volume of water	Irreducible water saturation
9697.5	8.63	8.54	0.01	8.72	76.29	35.68	20.89	52.14	0.19	2.34	−0.09	0.00	0.21	0.21	85.13	0.12	0.02	0.11
9697.75	8.63	8.56	0.00	8.92	75.98	35.96	20.27	61.13	0.19	2.34	−0.06	0.00	0.21	0.21	82.17	0.11	0.02	0.11
9698	8.63	8.58	0.00	9.12	75.67	36.23	19.65	70.12	0.18	2.34	−0.04	0.00	0.20	0.20	79.27	0.10	0.02	0.11
9698.25	8.63	8.59	0.00	8.41	75.76	35.17	20.01	96.38	0.18	2.33	−0.04	0.00	0.20	0.20	78.94	0.09	0.02	0.11
9698.5	8.63	8.59	0.00	7.70	75.85	34.11	20.37	122.64	0.17	2.33	−0.04	0.00	0.20	0.20	75.50	0.08	0.02	0.11
9698.75	8.63	8.60	0.00	6.99	75.94	33.05	20.73	148.90	0.17	2.33	−0.03	0.00	0.20	0.20	76.52	0.07	0.01	0.11
9699	8.63	8.60	0.01	6.29	76.03	31.99	21.09	175.16	0.18	2.33	−0.03	0.00	0.20	0.20	77.60	0.06	0.01	0.11
9699.25	8.63	8.60	0.01	6.08	75.49	29.79	20.64	140.03	0.18	2.32	−0.03	0.00	0.21	0.21	85.52	0.07	0.01	0.11
9699.5	8.63	8.60	0.00	5.88	74.95	27.58	20.19	104.89	0.18	2.32	−0.03	0.00	0.21	0.21	89.76	0.08	0.02	0.11
9699.75	8.63	8.59	0.00	5.68	74.41	25.38	19.74	69.76	0.18	2.31	−0.03	0.00	0.21	0.21	96.59	0.10	0.02	0.10
9700	8.63	8.59	0.00	5.48	73.87	23.18	19.29	34.63	0.19	2.31	−0.04	0.00	0.22	0.22	104.53	0.13	0.03	0.10
Average												0.01	0.22	0.22	113.26	0.14	0.03	0.10

$$S_{w} = \left\{ \left[\left(\frac{V_{sh}^{2-V_{sh}}}{R_{sh}} \right)^{1/2} + \left(\frac{\phi_{e}^{m}}{R_{w}} \right)^{1/2} \right]^{2} R_{t} \right\}^{-1/n} \tag{4}$$

where S_{w} water saturation; V_{sh} shale volume; ϕ_{e} effective porosity; R_{sh} shale resistivity; R_{t} deep resistivity; R_{w} connate water resistivity and set equals 0.03 Ω m²/m; m cementation exponent and set equals 2; n saturation exponent and set equals 2; a tortuosity factor and set equals 1.

The calculated water saturation is presented in track ten in Figs. 4 and 5 with blue colour, while green colour in the same column refers to the hydrocarbon saturation. The calculated water saturation is 39% in zone II (i.e. the hydrocarbon saturation equals 61%), while water saturation was lower in zone I and reaches only 13% (i.e. the hydrocarbon saturation equals 87%).

Figure 11 presents water saturation–effective porosity plot for the zones of interest. These plots obviously display that zone I is the best promising zone to be potential hydrocarbon reservoir since it has the highest ϕ_{e} and lowest S_{w} rather than zone II.

Bulk volume of water (BVW)

BVW has also been calculated for the interesting zones by applying the following equation (Buckles 1965):

$$BVW = \phi_{e} * S_{w} \tag{5}$$

where ϕ_{e} effective porosity; S_{w} water saturation.

The calculated BVW has been presented in track eleven in Figs. 4 and 5 and coloured with blue colour. The maximum bulk volume of water (0.06) was documented in in zone II, and the minimum value (0.03%) was noted in in zone I. Accordingly, zone I is predictable to produce water-free hydrocarbon rather than zone II.

Relative permeability and water cut

The hydrocarbon reservoir performance and the expected fluid through production step can be judged based on different measurements including relative permeability to oil K_{ro}, relative permeability to water K_{rw} and water cut Wc. These parameters depend on by the value of irreducible water saturation S_{wirr}. S_{wirr} has been calculated for the examined zones (see Tables 1 and 2) by the next formula:

$$S_{wirr} = (F/2000)^{0.5} \tag{6}$$

where S_{wirr} irreducible water saturation; F formation factor.

Since, $F = 1/\Phi^{2}$ (7)

where F formation factor; Φ porosity.

Table 2 Well-log data and output results for zone II in AG-15 Well

	Input well log data										Output results							
Depth (ft)	Bit size (IN)	Caliper (IN)	Density correction (G/C3)	Gamma ray (API)	Sonic (US/F)	Shallow resistivity (Ωm2/m)	Medium resistivity (Ωm2/m)	Deep resistivity (Ωm2/m)	Neutron porosity	Density (G/C3)	CALI-BS	Shale volume	Total porosity	Effective porosity	K (mD)	Water Saturation	Bulk volume of water	Irreducible water saturation
9962	8.50	8.80	0.04	23.04	83.20	8.95	3.81	3.84	0.18	2.35	0.30	0.14	0.20	0.16	23.40	0.53	0.08	0.14
9962.5	8.50	8.78	0.04	22.29	83.43	8.94	4.42	4.43	0.17	2.34	0.28	0.14	0.20	0.16	25.49	0.48	0.08	0.14
9963	8.50	8.76	0.04	21.35	83.09	9.14	4.76	5.33	0.17	2.34	0.26	0.13	0.20	0.16	28.35	0.43	0.07	0.14
9963.5	8.50	8.74	0.04	20.30	83.24	8.50	4.95	5.93	0.18	2.35	0.24	0.11	0.20	0.16	29.78	0.41	0.07	0.14
9964	8.50	8.72	0.04	19.49	84.00	7.83	4.96	6.17	0.18	2.38	0.22	0.11	0.19	0.16	23.99	0.42	0.07	0.14
9964.5	8.50	8.70	0.04	19.47	83.40	7.72	4.86	6.24	0.18	2.38	0.20	0.11	0.19	0.16	24.51	0.42	0.07	0.14
9965	8.50	8.67	0.04	19.47	81.95	6.76	4.66	6.16	0.17	2.40	0.17	0.11	0.18	0.15	17.83	0.45	0.07	0.15
9965.5	8.50	8.68	0.03	20.45	81.34	6.67	4.66	5.97	0.16	2.45	0.18	0.12	0.16	0.12	8.72	0.53	0.07	0.18
9966	8.50	8.69	0.02	21.32	80.11	7.07	4.76	5.92	0.16	2.46	0.19	0.13	0.15	0.12	6.56	0.56	0.06	0.19
9966.5	8.50	8.71	0.02	22.05	76.32	8.06	5.03	5.92	0.16	2.42	0.21	0.13	0.17	0.13	9.40	0.52	0.07	0.18
9967	8.50	8.72	0.02	21.85	74.62	9.55	5.44	6.10	0.17	2.37	0.22	0.13	0.19	0.15	19.46	0.44	0.07	0.15
9967.5	8.50	8.73	0.02	20.65	76.39	10.32	6.07	6.82	0.18	2.33	0.23	0.12	0.21	0.17	37.12	0.36	0.06	0.13
9968	8.50	8.74	0.02	19.73	79.25	11.10	6.32	7.76	0.18	2.30	0.24	0.11	0.22	0.18	49.75	0.32	0.06	0.12
9968.5	8.50	8.75	0.02	19.49	82.52	10.12	6.53	8.34	0.18	2.32	0.25	0.11	0.21	0.18	44.99	0.32	0.06	0.12
9969	8.50	8.76	0.02	20.48	81.64	8.16	6.91	8.53	0.18	2.32	0.26	0.12	0.21	0.18	41.08	0.32	0.06	0.13
9969.5	8.50	8.77	0.02	20.25	80.93	8.82	7.56	8.84	0.18	2.32	0.27	0.11	0.21	0.18	39.77	0.31	0.06	0.13
9970	8.50	8.78	0.02	19.87	81.13	11.33	8.14	9.76	0.18	2.33	0.28	0.11	0.21	0.17	39.53	0.30	0.05	0.13
9970.5	8.50	8.80	0.03	19.87	80.25	10.63	7.93	10.31	0.18	2.32	0.25	0.11	0.21	0.17	38.80	0.29	0.05	0.13
9971	8.50	8.81	0.03	20.50	79.55	10.44	7.77	10.86	0.17	2.34	0.31	0.12	0.20	0.16	29.87	0.30	0.05	0.14
9971.5	8.50	8.82	0.04	21.13	79.91	10.12	7.57	11.22	0.18	2.34	0.32	0.12	0.20	0.17	31.38	0.29	0.05	0.13
9972	8.50	8.83	0.05	22.51	79.07	8.47	7.53	11.42	0.18	2.33	0.33	0.14	0.20	0.16	28.58	0.29	0.05	0.14
9972.5	8.50	8.84	0.07	24.82	79.45	7.67	7.53	10.19	0.17	2.34	0.34	0.16	0.20	0.15	19.55	0.33	0.05	0.15
9973	8.50	8.85	0.09	29.16	80.27	9.66	7.55	9.19	0.16	2.35	0.35	0.21	0.19	0.13	9.81	0.39	0.05	0.18
Average												0.13	0.20	0.16	27.29	0.39	0.06	0.14
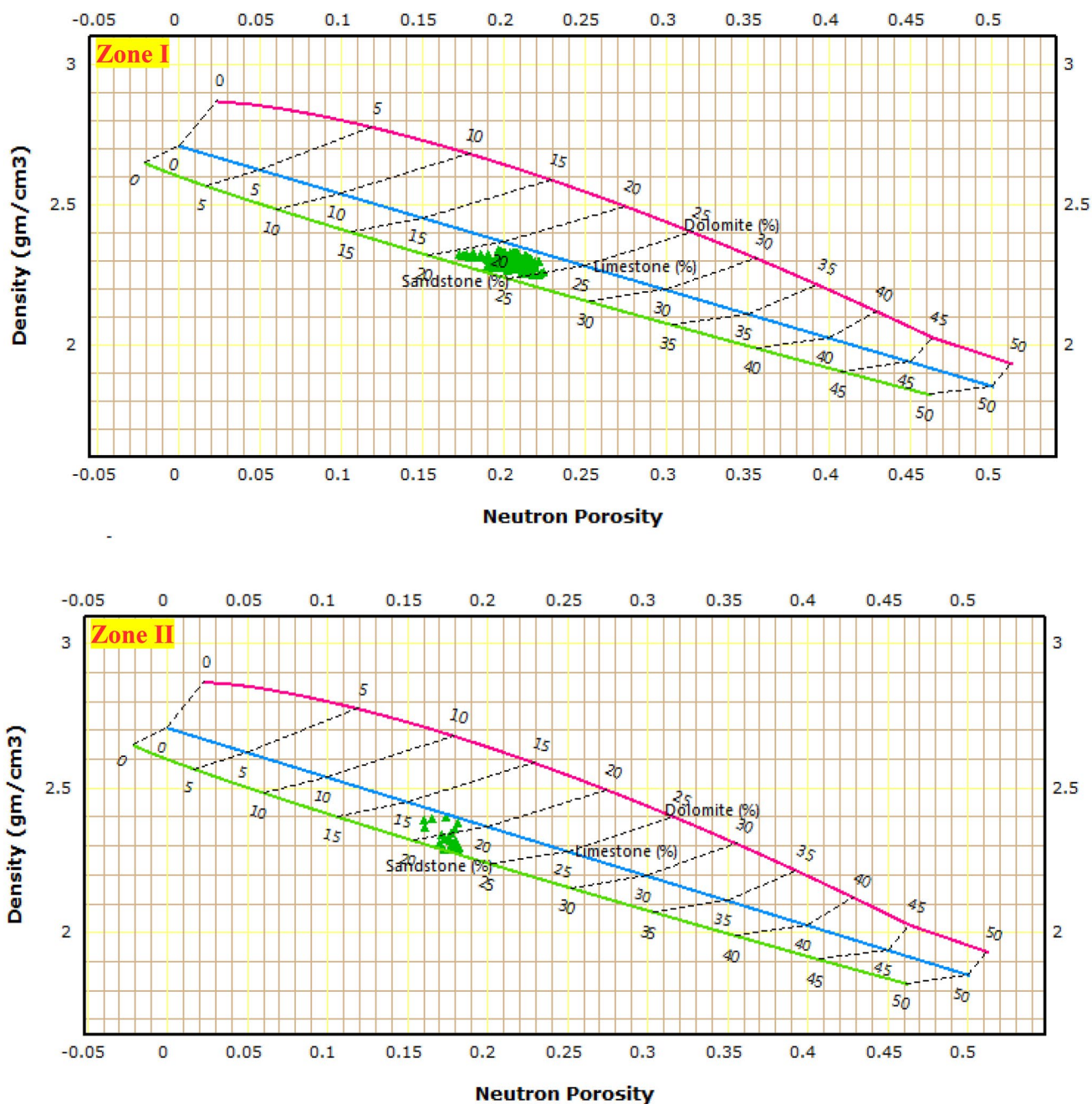
Fig. 9 Density–neutron plots (after Schlumberger 1972) for the examined zones within Abu Roash Fm. at Abu Gharadig Field

Several plots display the relation between S_w and S_{wirr} for the examined zones (have been created after Asquith and Gibson 1982) to judge the reservoir superiority of the Abu Roash C and E members in Abu Gharadig Field in the inspected wells. These plots indicate that zone I is the best oil-bearing interval since most plotted points locate: on and above $k_{ro} = 1$ (Fig. 12), on and below $k_{rw} = 0$ (Fig. 13) and below W_c of 20% (Fig. 14). However, zone II displays lower efficiency in the reservoir characteristics since most plotted

points locate between 0.5 and 0.1 k_{ro} (Fig. 12), between 0.01 and 0.1 k_{rw} (Fig. 13) and above W_c of 20% (Fig. 14). Moreover, the hydraulic characteristics in zone I are better than zone II. This is because the r35 value (Winland, 1972 and 1976) exceeds 5µ reflecting better flow quality than zone II which has r35 lower than 5µ (Fig. 15).

The gained results from this study have been proved by the obtainable information from the composite log and the drill-stem tests (DST) for AG-6 Well. The composite
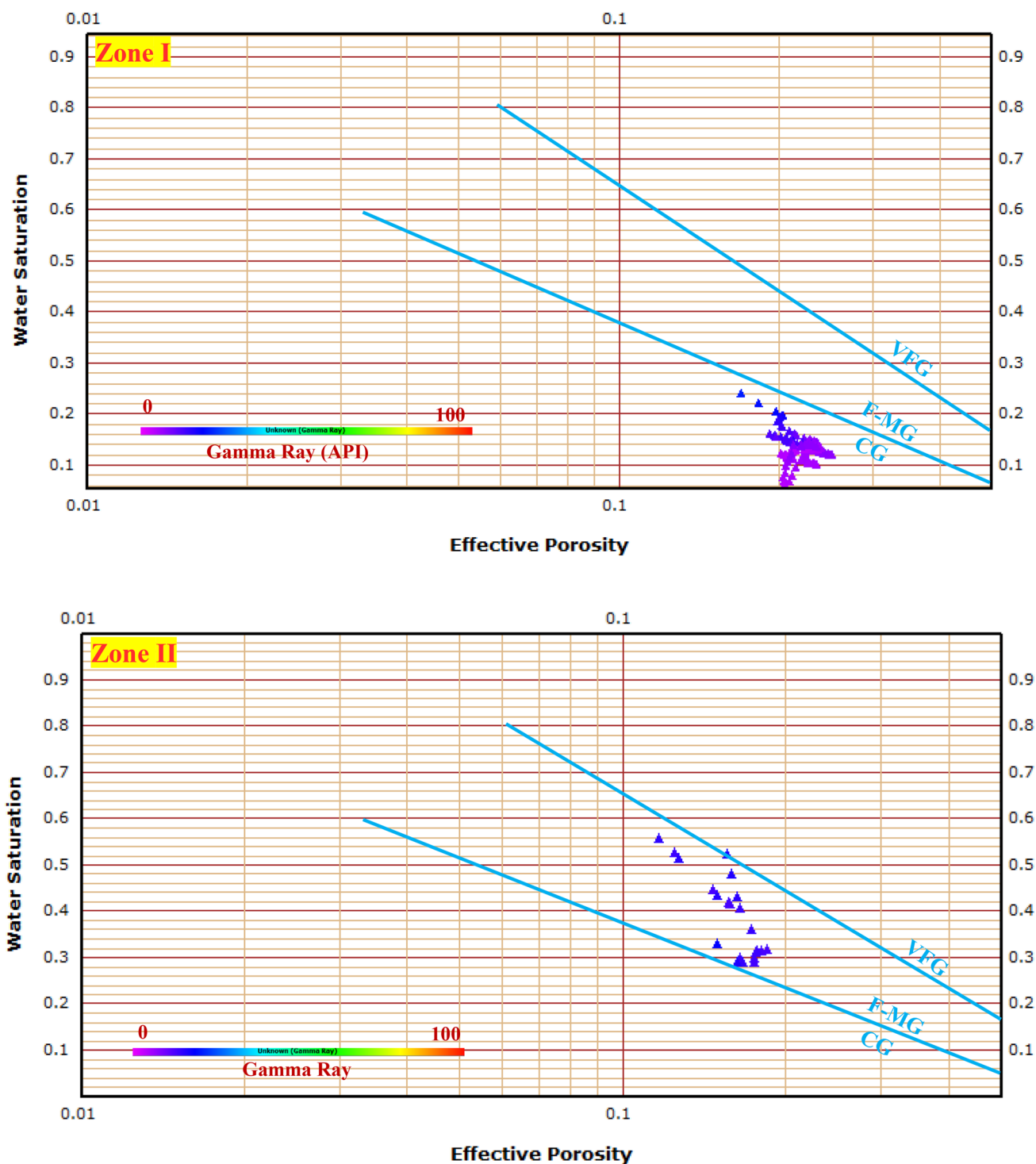
Fig. 10 Water saturation–effective porosity plots (Asquith and Gibson 1982) shows grain size distribution for the investigated zones within Abu Roash Fm. at Abu Gharadig Field

log shows oil satin and displays florescence opposite zone I. Moreover, the DST for zone I confirmed the production of 3744 BOPD with oil of 39.5° API plus 0.8 MMCFGPD. On the other hand, the drill-stem tests for zone II in AG-15 well proved the production of condensate with 49 API.
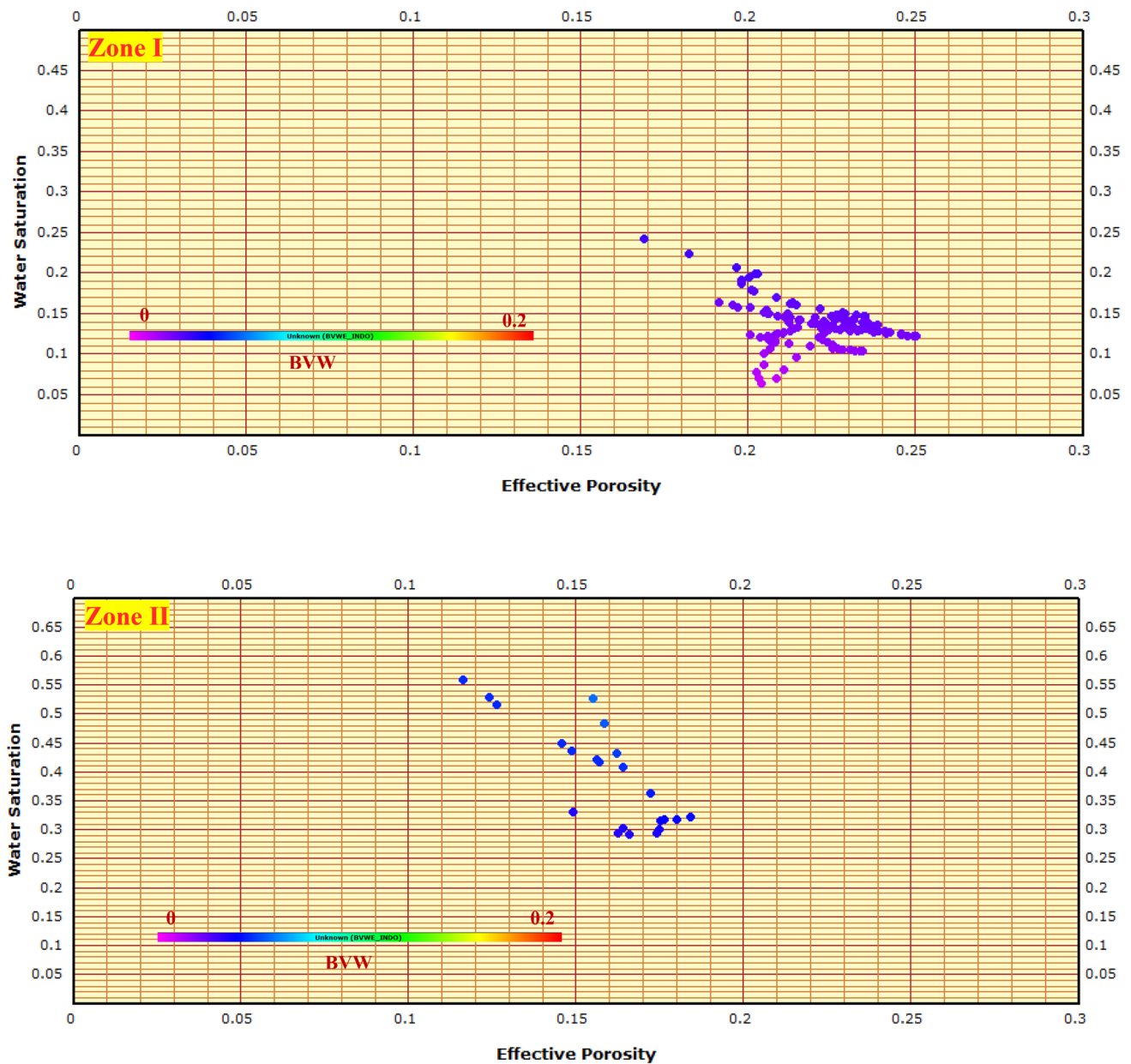
Fig. 11 Water saturation–effective porosity plots display the investigated zones within Abu Roash Fm. at Abu Gharadig Field

Conclusion

The conclusions reached in this paper are of significance to explorationists working both in Abu Gharadig Field and in the north Western Desert as follows:

- The Late Cretaceous dextral wrench corridor strongly affected the structural setting of north Western Desert including AG Basin. This was proven in this work through the seismic interpretation of Abu Gharadig Field which indicated the presence of ENE-WSW

Fig. 12 Water saturation—irreducible water saturation plots (Asquith and Gibson 1982) for evaluating the relative permeability to oil in the examined zones
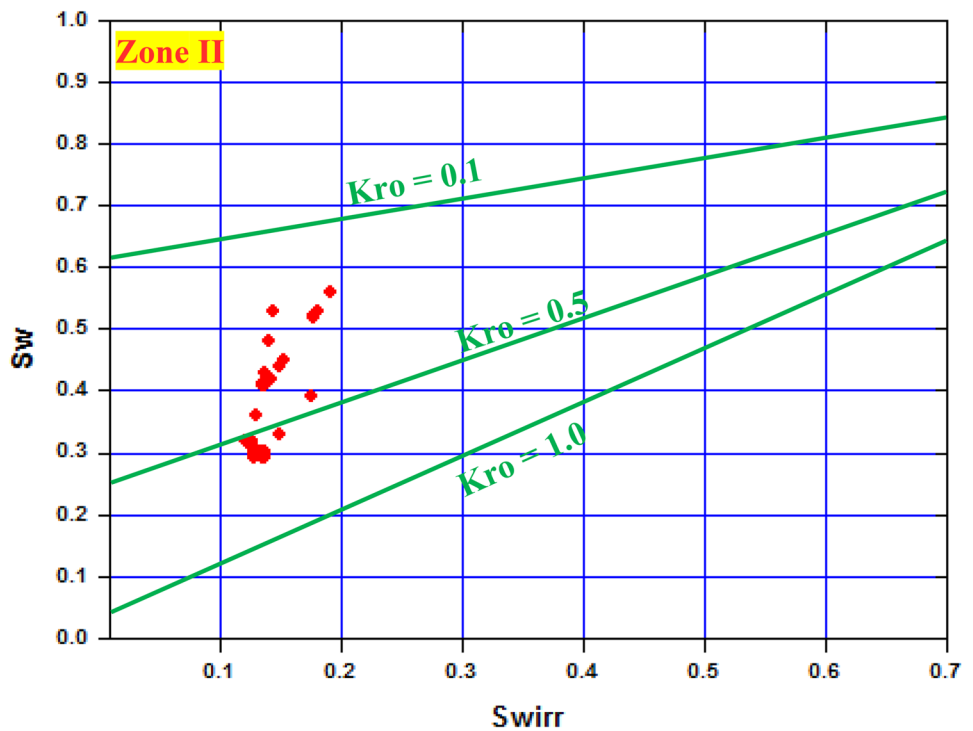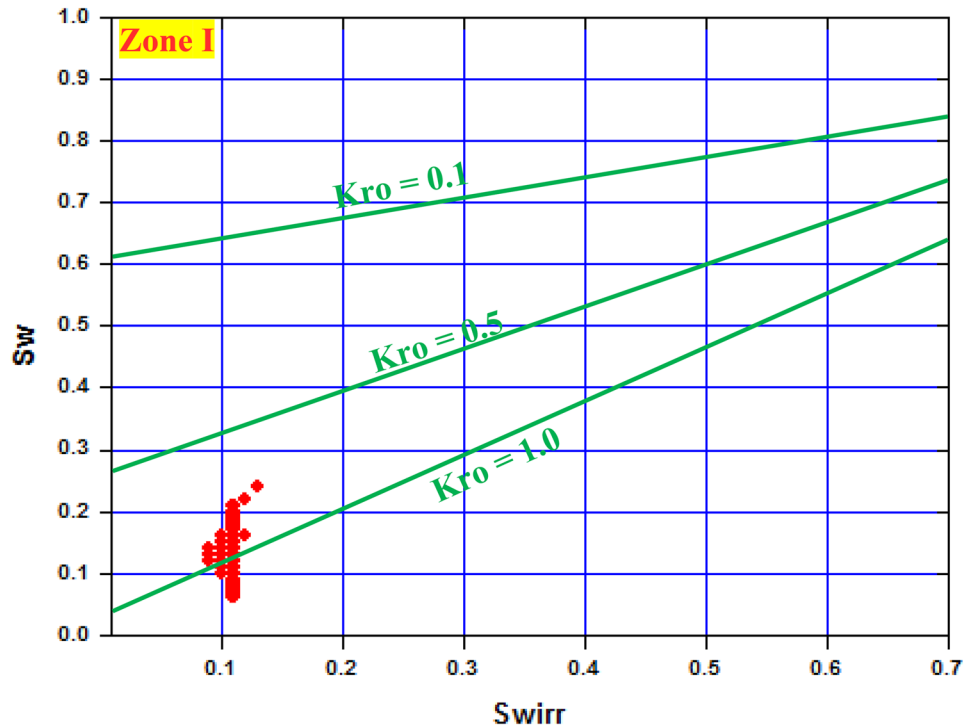
anticline disconnected by NW–SE normal faults reflecting the effect of this wrench. Consequently, the tectonic and structural settings of Abu Gharadig Field represent clear geological analogue for the exploration activity in other parts located at northern Western Desert where the Late Cretaceous dextral wrench-

Fig. 13 Water saturation—irreducible water saturation plots (Asquith and Gibson 1982) for assessing the relative permeability to water for the zones of interest
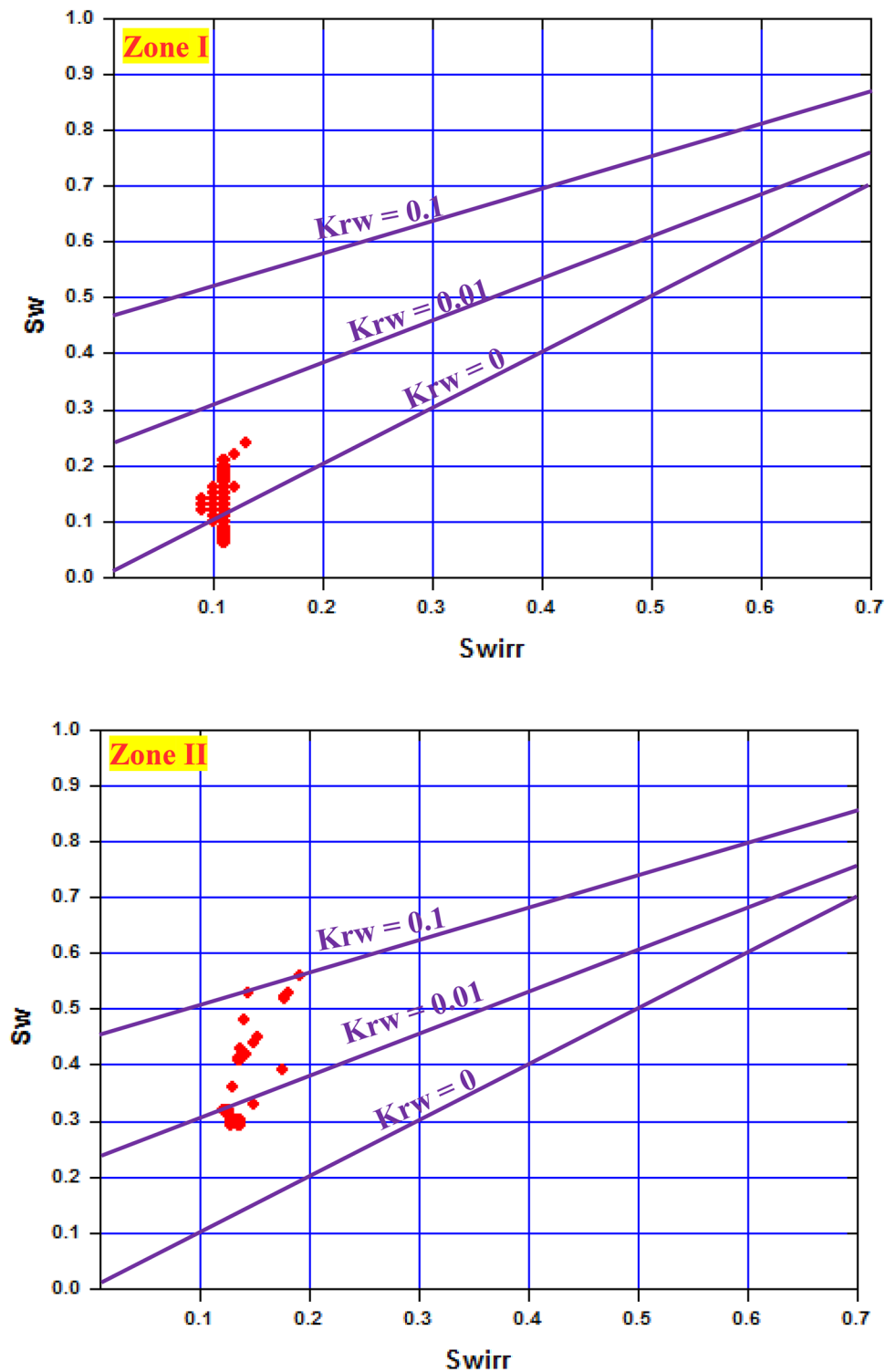
ing influences the distribution of other hydrocarbon fields.

- The comparison between the petrophysical parameters for the sandstones of Abu Roash C and E members in

Abu Gharadig Field revealed good reservoir characteristics in the sands of Abu Roash C Member rather than Abu Roash E Member. Accordingly, for further devel-

Fig. 14 Water saturation—irreducible water saturation plots (Asquith and Gibson 1982) to calculate the water-cut percentage for the interesting zones
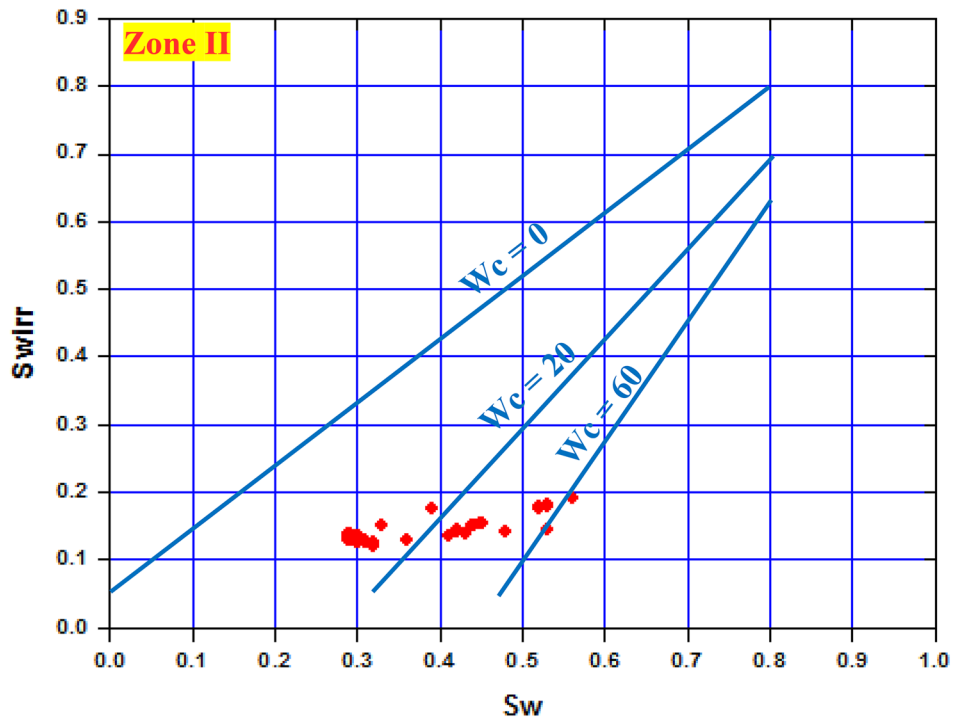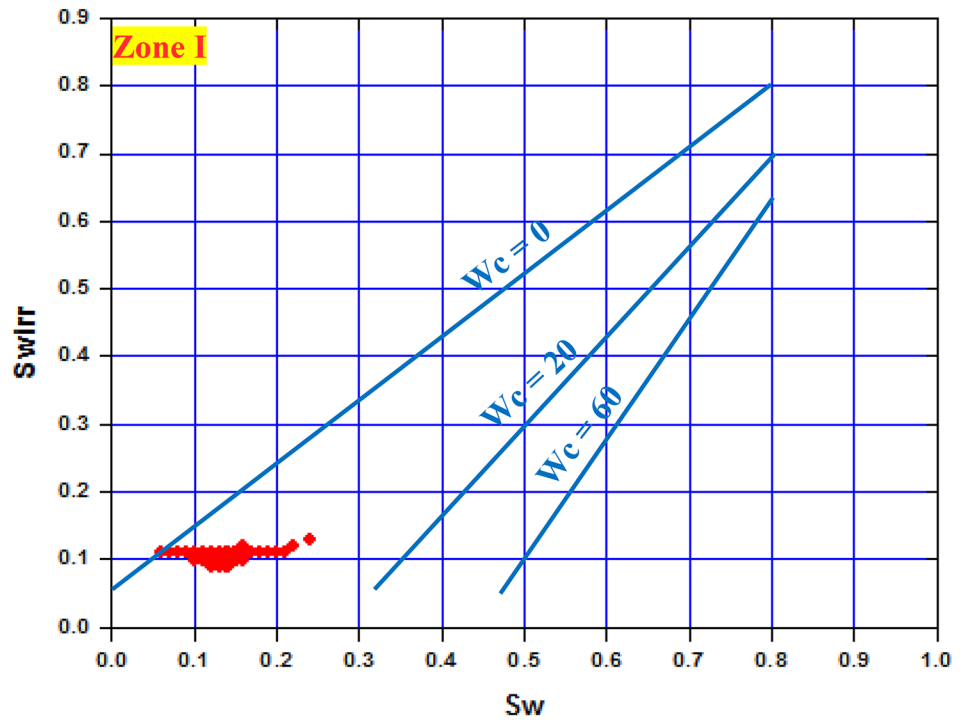
opment of the present hydrocarbon accumulations or for the exploration of new prospects in AG Basin and its surroundings, the efforts should be focused on the sandy levels within Abu Roash C Member (1st priority) and the sand levels within Abu Roash E Member (2nd priority).
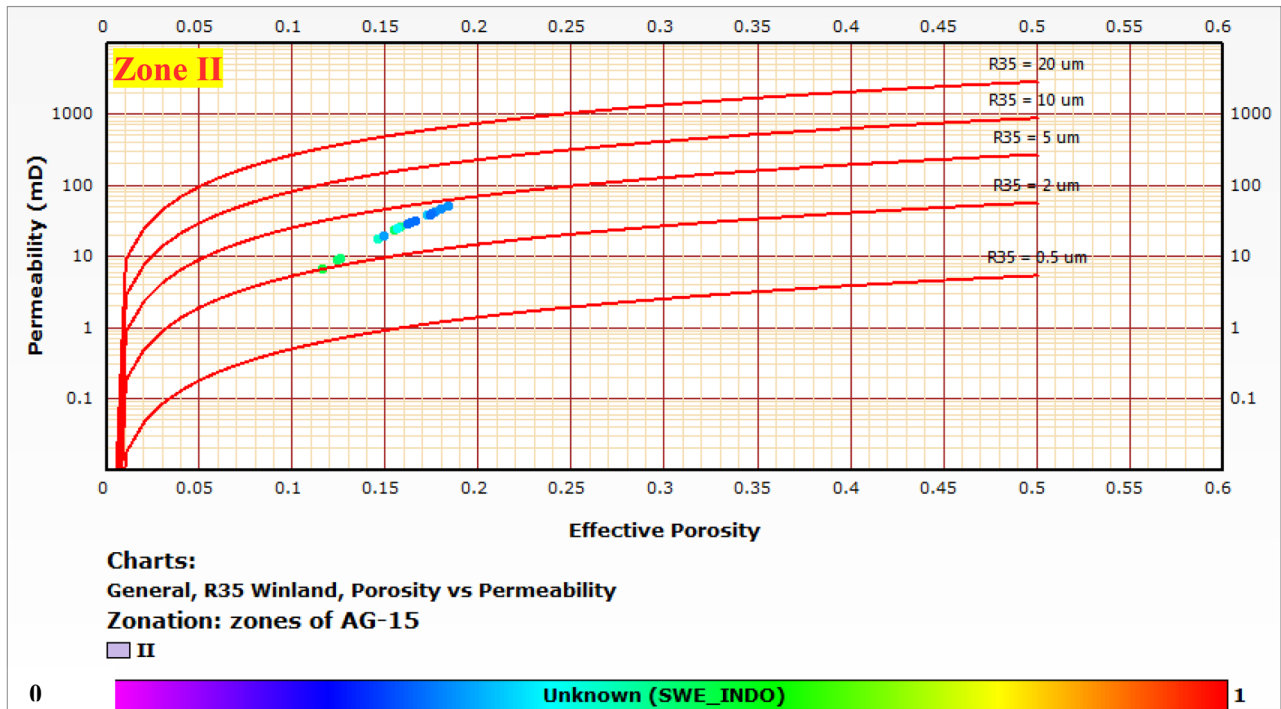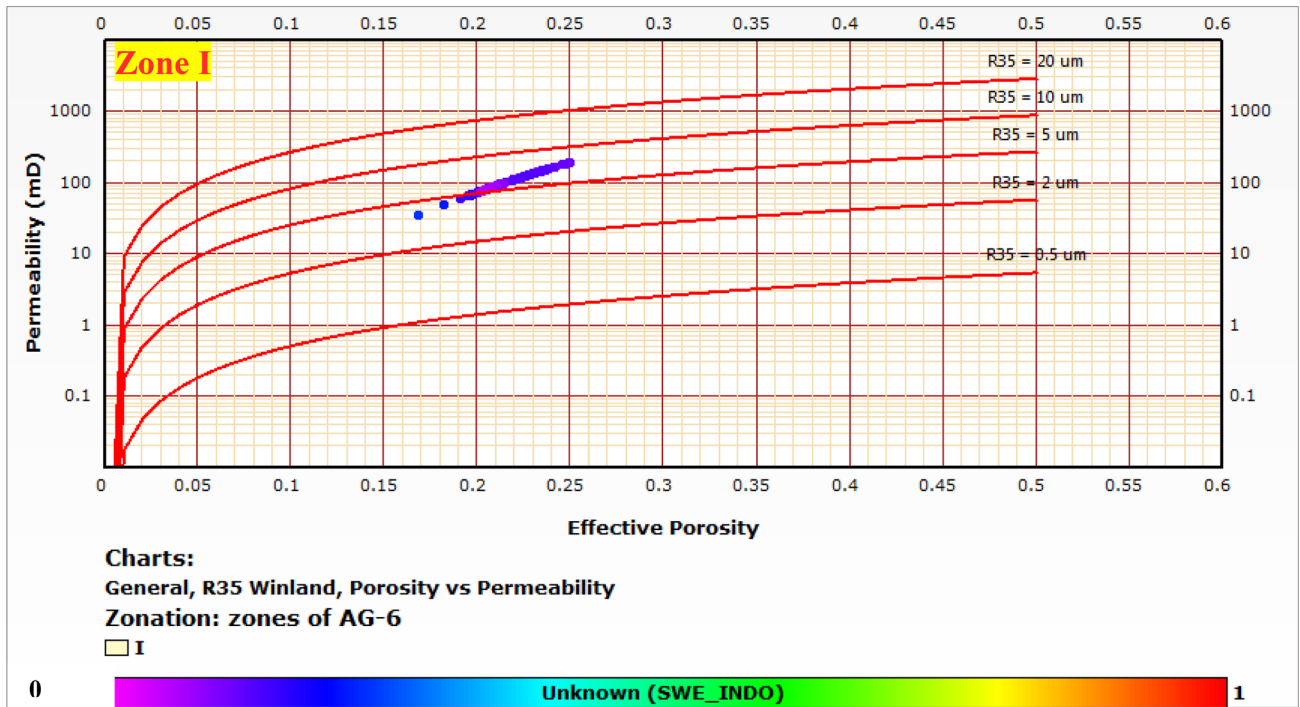
Fig. 15 Correlation graph (Y-axis signifies the permeability values; X-axis characterises the effective porosity values and the colour reflects the water saturation values) signifies the r35 value (Winland, 1972 and 1976). Note that this figure is just a representative graph for correlation between zones I and II since the plotted points are not based on microscopic measurements of rock core samples

References

Abd El Aal A (1988) In structural framework of AG Basin Western Desert, Egypt. 9th petroleum exploration and production conference. Egyptian General Petroleum Corporation, Cairo, pp 20–23

Abd El Aal A, Moustafa AR (1988) Structural framework of the AG Basin, Western Desert, Egypt. Paper presented at the 9th exploration and production conference, vol 2. Egyptian General Petroleum Corporation, Cairo, pp 23–50

Abu El Naga M (1984) In paleozoic and mesozoic depocenters and hydrocarbon generating areas, northern Western Desert. 7th petroleum and exploration seminar, vol 8. Egyptian General Petroleum Corporation, Cairo, pp 269–287

Asquith G, Gibson C (1982) Basic well log analysis for geologists: methods in Exploration series. AAPG, Tulsa, Oklahoma

Barakat MK, Nooh AZ (2017) Reservoir quality using the routine core analysis data of Abu Roash "C" in Badr El Din-15 oil field, AG Basin, north Western Desert, Egypt. J Afr Earth Sci 129:683–691

Biju-Duval B, Dercourt J, Le Pichon X (1977) From the Tethys ocean to the Mediterranean seas: a plate tectonic model of the evolution of the western Alpine system. In: Biju-Duval B, Montadert L (eds) Structural history of the mediterranean basins. Editions Technip, Paris, pp 143–164

Bosworth W, El-Hawat AS, Helgeson DE, Burke K (2008) Cyrenaican "shock absorber" and associated inversion strain shadow in the collision zone of northeast Africa. Geology 36(9):695–698

Buckles RS (1965) Correlating and averaging connate water saturation data. J Can Pet Technol 4(1):42–52

Dolson CJ, Shaan VM, Matbouly S, Harwood C, Rashed R, Hammouda H (2001) The petroleum potential of Egypt. In: Downey WM, Threet CJ, Morgan AW (eds) Petroleum provinces of the twenty-first century, vol 74. American Association of Petroleum Geologists (AAPG), Tulsa, pp 453–482

EGPC (1992) Western Desert, oil and gas fields, a comprehensive overview. 11th petroleum exploration and production conference. Egyptian General Petroleum Corporation, Cairo, pp 1–431

El Diasty WS, Moldowan JM (2012) Application of biological markers in the recognition of the geochemical characteristics of some crude oils from AG Basin, north Western Desert-Egypt. Mar Pet Geol 35(1):28–40

El Gezeery NH, and O' Connor T (1975) Cretaceous rock units in the Western Desert, Egypt. In: 13th annual meeting of geological society of Egypt. Geological Society, Cairo, p. 2

El Gazzar AM, Moustafa AR, Bentham P (2016) Structural evolution of the Abu Gharadig field area, northern Western Desert. Egypt J Afr Earth Sci 124:340–354

El Sayed AMA, Mouse SA, Higazi A, Al-Kodsh A (1993) Reservoir characteristics of the Bahariya formation in both Salaam and Khalda oil fields, Western Desert, Egypt. EGS Proc Ann Mtg 11:115–132

El-Bagoury M (2020) Integrated petrophysical study to validate water saturation from well logs in Bahariya Shaley Sand Reservoirs, case study from AG Basin, Egypt. J Pet Exploration and Prod Technol 1–17

Elmahdy M, Tarabees E, Farag AE, Bakr A (2020) An integrated structural and stratigraphic characterization of the Apollonia carbonate reservoir, Abu El-Gharadig Basin, Western Desert Egypt. J Nat Gas Sci Eng 78:103317

Guiraud R, Bosworth W (1997) Senonian basin inversion and rejuvenation of rifting in Africa and Arabia: synthesis and implications to plate-scale tectonics. Rev Tectonophys 282:39–82

Hewaidy AG, Elshahat OR, Kamal S (2018) Stratigraphy, facies analysis and depositional environments of the upper unit of Abu Roash "E" member in the Abu Gharadig field, Western Desert. Egypt J Afr Earth Sci 139:26–37

Labib M (1985) Contributions to the geology of upper cretaceous with special emphasis on Turonian–Senonian sedimentation patterns and hydrocarbon potentialities in the Abu Gharadig area, north Western Desert, Egypt. In: Unpublished dissertation thesis, geology department. Cairo University, Cairo, p 189

Meshref WM, Abu El Karamat MS, El Gindi MK (1988). Exploration concepts for oil in the Gulf of Suez vol 1. In: Paper presented at the 9th exploration and production conference, EGPC, Cairo 1–23.

Moustafa, A. R. (2002). Structural style and timing of Syrian arc deformation in northern Egypt. Am Assoc Petrol Geol Int Meeting

Moustafa AR (2008) Mesozoice cenozoic basin evolution in the northern Western Desert of Egypt. In: Salem M, El-Arnauti A, Saleh A (Eds), 3rd symposium on the sedimentary basins of libya vol 3. The Geology of East Libya, pp 29–46

Moustafa AR, Khalil MH (1990) Structural characteristics and tectonic evolution of north Sinai fold belts. In: Said R (ed) The geology of Egypt. A. A. Balkema Publishers, Rotterdam, Netherlands, pp 381–392

Moustafa AR, Badrawy RE, Gibali H (1998) Pervasive E-ENE oriented faults in Northern Egypt and their effect on the development and inversion of prolific sedimentary basins. In: Eloui M (ed) 14th petroleum conference. The Egyptian General Petroleum Corporation, Cairo, Egypt, pp 51–67

Poupon A, and Leveaux J (1971) Evaluation of water saturation in shaly formations. In: SPWLA 12th annual logging symposium. Society of Petrophysicists and Well-Log Analysts, Oklahoma

Richardson MS, Vivian N, Cook JR, Wilkes M, Hussein H (1998) Application of fault seal analysis techniques in the Western Desert, Egypt. In: Macgregor SD, Moody JTR, Clark Lowes DD (eds) Petroleum geology of North Africa. Geological Society of London, Special Publication, pp 297–315

Robertson Research International (RRI) (1985). Further evaluation of the Abu Sennan–Alam El Shawish area, Western Desert, the Arab Republic of Egypt, with emphasis on stratigraphic trapping potential

Sarhan MA (2017a) Seismic-wireline logs sequence stratigraphic analyses and geologic evolution for the upper cretaceous succession of AG Basin. Egypt J Afr Earth Sci 129:469–480

Sarhan MA (2017b) Wrench tectonics of AG Basin, Western Desert, Egypt: a structural analysis for hydrocarbon prospects. Arab J Geosci 10(18):399

Sarhan MA (2017c) The efficiency of seismic attributes to differentiate between massive and non-massive carbonate successions for hydrocarbon exploration activity. NRIAG J Astron Geophys 6(2):311–325

Sarhan MA (2020) Possibility of intrusive igneous body beneath the cretaceous sequence in AG Basin, Egypt: integration of geophysical data interpretations. Arab J Geosci 13(12):1–10

Sarhan MA, Basal AMK (2020) Total organic carbon content deduced from resistivity-porosity logs overlay: a case study of Abu Roash formation, Southwest Qarun field, Gindi Basin. Egypt NRIAG J Astron Geophys 9(1):190–205

Sarhan MA, Collier REL (2018) Distinguishing rift-related from inversion-related anticlines: observations from the Abu Gharadig and Gindi Basins, Western Desert. Egypt J Afr Earth Sci 145(2018):234–245

Sarhan MA, Basal AMK, Ibrahim IM (2017) Integration of seismic interpretation and well logging analysis of Abu Roash D Member, Gindi Basin, Egypt: Implication for detecting and evaluating fractured carbonate reservoirs. J Afr Earth Sci 135:1–13

Schlumberger (1972) Log interpretation/charts. Schlumberger Well Services Inc, Houston

Sestini, G. (1995). Egypt. In: Kulke, H. (Ed.), Regional petroleum geology of the world, part II: Africa, America, Australia and Antarctica vol. Beiträge zur regionalen Geologie der Erde, Gebrüder Bornträger Verlagsbuchhandlung, Stuttgart. Band 22 pp 66–87.

Shahin AN (1992) In Undiscovered petroleum reserves in North Western Desert, Egypt. Paper presented at the 1st Int. Confer. Geology of Arab World, GUPCO, Cairo University

Smith AG (1971) Alpine deformation and the oceanic areas of the Tethys, Mediterranean, and Atlantic. Geol Soc Am Bull 82(8):2039–2070

Sultan N, Abd El Halim M (1988) In tectonic framework of Northern Western Desert, Egypt and its effect on hydrocarbon accumulations. Paper presented at the 8th exploration and production conference. Egyptian General Petroleum Corporation, Cairo, pp 20–23

Winland HD (1972) Oil accumulation in response to pore size changes, Weyburn field, Saskatchewan: Amoco Production Company Report F72-G-25, 20 p (unpublished)

Winland HD (1976) Evaluation of gas slippage and pore aperture size in carbonate and sandstone reservoirs: Amoco Production Company Report F76-G-5, 25, p (unpublished)

Wyllie MRJ, Rose WD (1950) Some theoretical considerations related to the quantitative evaluation of the physical characteristics of reservoir rock from electrical log data. J Petrol Technol 2(04):105–118